www.acsnano.org

Synthesis of Ternary and Quaternary Group III-Arsenide Colloidal Quantum Dots via High-Temperature Cation Exchange in Molten Salts: The Importance of Molten Salt Speciation

Justin C. Ondry, Aritrajit Gupta, Zirui Zhou, Jun Hyuk Chang, and Dmitri V. Talapin*



Downloaded via UNIV OF CHICAGO on January 2, 2024 at 22:37:18 (UTC). See https://pubs.acs.org/sharingguidelines for options on how to legitimately share published articles.

Cite This: https://doi.org/10.1021/acsnano.3c09490



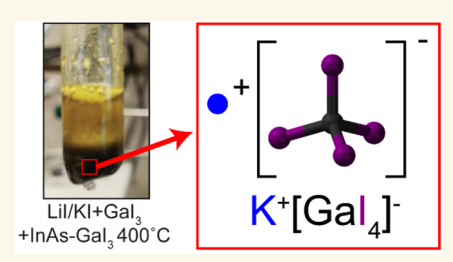
ACCESS I

III Metrics & More

Article Recommendations

S Supporting Information

ABSTRACT: Colloidal semiconductor nanocrystals are an important class of materials which have many desirable optoelectronic properties. In their bulk phases, gallium- and aluminum-containing III–V materials such as GaAs, GaP, and $Al_{1-x}Ga_xAs$ represent some of the most technologically important semiconductors. However, their colloidal synthesis by traditional methods is difficult due to the high temperatures needed to crystallize these highly covalent materials and the extreme reactivity of Ga- and Al- precursors toward organic solvents at such high temperatures. A recently developed paradigm shift in the synthesis of these materials is to use molten inorganic salts as solvents to prepare Ga- containing III–



V colloidal nanocrystals by cation exchange of the corresponding indium pnictide (InPn) colloidal nanocrystals. There have been several successful applications of molten salt solvents to prepare III-phosphide colloidal nanocrystals. However, little is known about the nature of these reaction environments at the relevant reaction conditions and synthesis of III-arsenide colloidal nanocrystals remains challenging. Herein we report a detailed study on cation exchange of InPn nanocrystals using nominally Lewis basic molten salt solvents with added gallium halides. Surprisingly, these salt systems phase separate into two immiscible phases, and the nanocrystals preferentially segregate to one of the phases. Using a suite of *in situ* spectroscopy tools, we identify the phase the nanocrystals segregate to as Lewis neutral alkali tetrahalogallate molten salts. We apply *in situ* high-temperature Raman spectroscopy to identify the chemical species present in several molten salts. We apply *in situ* high-temperature Raman spectroscopy to identify the chemical species present in several molten salt compositions at experimentally relevant reaction conditions to elucidate a molecular basis for the reactivity observed. We then employ Lewis neutral KGaI₄ molten salts to prepare high-quality $In_{1-x}Ga_xAs$ and $In_{1-x}Ga_xP$ nanocrystals and demonstrate that deviation from Lewis neutral conditions accelerate nanocrystal decomposition in the case of III-arsenide materials. Further, we expand to KAII₄-based molten salts to prepare $In_{1-x-y}Ga_xAl_yAs$ nanocrystals which represent an example of solution-synthesized quaternary III-V nanocrystals. These insights provide a molecular basis for the rational development of molten salt solvents, thus allowing the preparation of a diverse array of multicomponent III-V colloidal nanocrystals.

KEYWORDS: Colloidal Nanocrystals, Molten Salt, Cation Exchange, Alloy Nanocrystals, III–V Nanocrystals

olloidal synthesis is a powerful methodology to prepare diverse materials as small (1–100 nm) crystallites which can be solution processed and integrated in various devices. Many key materials classes including technologically important metals, metal oxides, metal halides, metal chalcogenides, and metal pnictides can be synthesized as nanocrystals with exquisite control over size, shape, and phase, etc. Nanocrystals made of semiconducting materials are particularly intriguing for optoelectronic applications because they provide size-tunable electronic structures that can be exploited for a variety of practical applications, such as color converters for display applications and active materials for IR detectors.

Early approaches to prepare colloidal semiconductor nanocrystals (e.g., CdS, CdSe, etc.) were based on reactions inside reverse micelles where aqueous alkali chalcogenides were reacted with aqueous metal salts to produce size-controlled colloids. These methods were limited by the low growth temperatures resulting in poorly crystalline semiconductors

Received: September 29, 2023 Revised: December 6, 2023 Accepted: December 8, 2023



which contained many optically active defects and concomitantly low luminescence efficiency. Many of these limitations were overcome by the development of high-temperature organometallic synthesis routes for semiconductor nanocrystals. Through an appropriate selection of reagents and highboiling organic solvents, high-quality colloidal nanocrystals made of II-VI, IV-VI, and indium-V materials have been successfully synthesized. 11-13 For some classes of these materials, prodigious examples have achieved photoluminescence quantum yields (PL QY) indistinguishable from unity, 14,15 indicating that the materials produced are nearly free of deleterious defects. In general, for colloidal quantum dots, especially of the III-V semiconductors, higher growth temperatures lead to improved optoelectronic performance. Many state-of-the-art syntheses for II-VI and III-V materials operate above 300 °C and near the decomposition temperature of the solvents. 16 For some key materials, such as highly covalent GaAs, traditional organometallic synthesis routes have not yet achieved nanocrystals with band edge PL, 17-19 indicating that temperatures achievable with high-boiling organic solvents are insufficient to synthesize defect-free

One possible paradigm shift is to use a molten inorganic salt as a "solvent" (or "flux" in the solid-state chemistry vernacular) for colloidal synthesis since they have higher thermal, chemical, and electrochemical stability than their organic counterparts.^{20,21} Recent demonstration of stable nanocrystal colloids in molten salts presents many opportunities for synthesis and transformation of colloidal materials.²² Indeed, initial studies using molten salt solvents for chemical transformation of colloidal nanocrystals enabled reactions which had thus far not been possible with traditional organic solvents. For example, InP and InAs nanocrystals were transformed into their respective ternary alloys, In_{1-x}Ga_xP and In_{1-x}Ga_xAs by annealing the nanocrystals in a molten mixture of a low melting CsBr/KBr/LiBr eutectic and gallium iodide at temperatures from 380 to 500 °C. 23,24 In these reactions, the nanocrystals are stripped of their native organic ligands and are replaced with all inorganic ligands including III-halide salts, chalcogenide ligands or "bare" surfaces. Next, they are dispersed in the molten salt reaction medium and annealed at high temperature. To isolate the nanocrystals, the solidified salt matrix is dissolved in an appropriate solvent (formamide, acetonitrile, etc.) and the nanocrystals which are insoluble in the solvent, are recovered by centrifugation. Finally, the nanocrystals are made colloidal in organic solvents by addition of appropriate surface ligands (e.g., oleylamine, oleic acid, etc.) to regain colloidal stability. Importantly this methodology resulted in highly luminescent In_{1-x}Ga_xP/ZnS and In_{1-r}Ga_rAs/CdS nanocrystals demonstrating that molten salt derived colloidal nanocrystals have high crystal quality. Importantly, molten salt solvents are thus far the only route which has resulted in highly emissive Ga-containing III-V nanocrystals over a wide composition range. 25,26 Given the potential to prepare high-quality materials, it is imperative to better understand these unconventional reaction environments to enable rational design of molten salt derived colloidal materials.

Here we reevaluate the molten salt environments we previously developed for molten salt mediated cation exchange of III–V colloidal nanocrystals. We use *in situ* spectroscopy to identify KGaI₄ as the key chemical species which is active for gallium cation exchange in III–V nanocrystals. Next, we

demonstrate $KGaI_4$ engenders chemical stability of InAs and InP nanocrystals at high temperatures and show that deviation from the $KGaI_4$ composition leads to accelerated decomposition of III—V colloidal nanocrystals. We develop a relationship between the chemical species present in the salts at the reaction temperatures by performing in situ Raman spectroscopy and determine that the tetraiodogallate species remain well-defined even at elevated temperatures. Finally, based on the insights from the gallium halide molten salt solvents, we engineer aluminum halide molten salts which enable chemical stability of III—V nanocrystals in these reactive salts and demonstrate quaternary III—V phases including colloidal $In_{1-x-v}Ga_vAl_vAs$ nanocrystals.

RESULTS AND DISCUSSION

Molten Salt Chemistry Relevant to III–V Cation Exchange Reactions. Molten salts can be classified based on the Lewis acidity of the salt melt. Lewis basic salts (Scheme 1A) contain ions which are electron donors and the alkali

Scheme 1. Overview of Molten Salt Classes. (A) Lewis Basic Molten Salts Contain Ions Which Are Electron Donors (e.g., Cl⁻) and Typical Alkali Halide Eutectic Molten Salts Are Key Solvents in the Category. (B) Lewis Acidic Molten Salts Contain Species Which Are Strong Electron Acceptors (e.g., AlCl₃, [Al₂Cl₇]⁻). (C) Lewis Neutral Molten Salts Result from the Reaction of a Lewis Basic Component with a Lewis Acidic Component^a

A Lewis Basic B Lewis Acidic C Lewis Neutral KCI+AICI_3—KAICI_4
$$\begin{bmatrix} K^+ & CI^- & CI & KI/LiI \\ I & I & KI/LiI \\ I37:63 \text{ mol }\%] & G8B_1/KB_1/LiBr \\ C8B_1/KB_1/LiBr \\ [25:56:19 \text{ mol}\%] & KAII_4 \end{bmatrix}$$

"Lewis neutral salts do not contain any strongly coordinating species. In this work, we will focus on using KI/LiI [37:63 mol %] and CsBr/KBr/LiBr [25:56:19 mol %] as Lewis basic salts, GaI₃/KI [65:35 mol %] as a Lewis acidic molten salt, and KGaI₄ and KAII₄ as Lewis neutral molten salts.

halide eutectics are common examples. We have previously shown that the strong coordination of the halides to the nanocrystal surfaces in these salts are key to ensuring colloidal stability. Lewis acidic salts (Scheme 1B) contain molecules and ions which are electron acceptors and examples include GaI₃/KI [65:35 mol %] eutectic mixtures. In the molten state, Lewis acidic salt mixtures contain a complex mixture of different species including MX_3 , M_2X_6 , $[M_2X_7]^-$, $[MX_4]^-$ (M =Al, Ga, In; X = Cl, Br, I) depending on the composition and stoichiometry. Nanocrystals in Lewis acidic molten salts also display good colloidal stability owing to the strong interaction between the nanocrystal surface and the Lewis acidic species acting as Z-type ligands.²⁷ Reaction of equimolar amounts of Lewis acidic species and Lewis basic species according to the general reaction AX+MX₃→ AMX₄ results in Lewis neutral molten salts which have a molecular structure distinct from their parent compounds (Scheme 1C). Importantly these salts do not contain any strongly coordinating ions or molecular species. Without strongly coordinating ions, nanocrystals in Lewis neutral molten salts show reduced colloidal stability

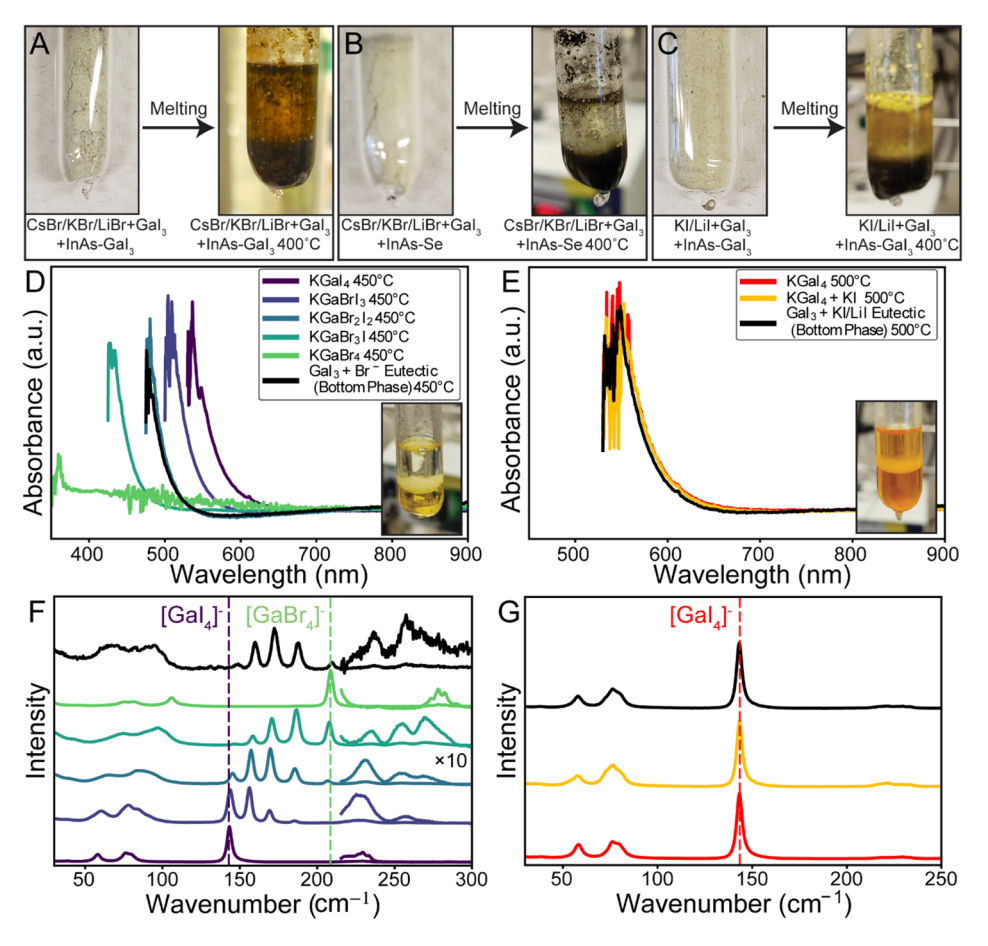


Figure 1. Photographs of a homogeneous mixture of finely ground (A) CsBr/KBr/LiBr eutectic salt (1 g), GaI₃ (500 mg), and InAs nanocrystals capped with GaI₃ (~50 mg) before melting (left) and after melting (right), (B) CsBr/KBr/LiBr eutectic salt (1g), GaI₃ (500 mg), and InAs nanocrystals capped with Se surface ligands (~50 mg) before melting (left) and after melting (right), and (C) KI/LiI eutectic salt (1 g), GaI₃ (500 mg), and InAs nanocrystals capped with GaI₃ surface ligands (~50 mg) before melting (left) and after melting (right). In situ UV—vis absorption spectra from the lower phase (see inset photo) compared to appropriate reference compounds for (D) GaI₃ added to the CsBr/KBr/LiBr eutectic and (E) GaI₃ added to the KI/LiI eutectic. The absorption spectra are not normalized in any way. (F, G) Room temperature Raman spectra of the lower salt phase compared with Raman spectra for the appropriate reference compounds for (F) GaI₃ added to the CsBr/KBr/LiBr eutectic and (G) GaI₃ added to the KI/LiI eutectic. Line colors are the same in panels D and F and in E and G.

compared to acidic and basic compositions. Importantly, the degree of Lewis acidity can be continuously tuned in molten salts, which in turn changes the species present and their relative concentrations. With this incredible tunability, molten salts have the potential to enable precision synthesis of colloidal nanomaterials.

Dispersion of Colloidal Nanocrystals in Gallium Halide Containing Molten Salts. The initial molten salt colloidal nanocrystal cation exchange reactions utilized a low melting Lewis basic alkali halide eutectic mixture (e.g., CsBr/ KBr/LiBr or KI/LiI) to disperse the nanocrystals as stable colloids in the molten salts. In the pure alkali halide molten salts, we observe highly stable colloids of InP and InAs NCs with all-inorganic surface terminations such as GaI₃²⁸ or Li₂Se²⁹ when the salts are melted. This observation is consistent with the principles of colloidal stability in the molten salt solvents we previously identified where Lewis basic molten salts provide colloidal stability to many nanocrystal compositions.27 For cation exchange, a gallium source is added in the form of gallium iodide to the nanocrystals dispersed in the alkali halide eutectic. Here the initial notion of this reaction environment was that the alkali halide molten salt simply provided universal cosolubility to the nanocrystals and gallium source. Based on the above discussion of Lewis acid-base chemistry of molten salts, we infer that the GaI₃ will convert to an alkali tetrahalogallate species consuming 1 equiv of AX from the Lewis basic eutectic. We empirically found that a large excess of GaI3 was needed for the reactions to work, and addition of stoichiometric equivalents of gallium halide relative to the number of indiums present in the nanocrystals were unsuccessful. Further, we empirically observed degraded colloidal stability of the nanocrystals upon addition of the gallium iodide to the colloidal solution of InAs or InP nanocrystals in the alkali halide molten salt. Despite the apparently degraded colloidal stability, these reaction environments enabled the synthesis of high-quality In_{1-x}Ga_xP colloidal nanocrystals which show strong band-edge PL once a ZnS shell is deposited to passivate surface traps. These observations demonstrate the potential of molten salt solvents for colloidal synthesis; however, a precise understanding of the molten salt reaction environment remains elusive.

To better understand the colloidal stability of nanocrystals in GaI₃ containing alkali halide eutectic salts, we prepared large-scale mixtures of finely coground alkali halide eutectic salt,

GaI₃, and InAs nanocrystals, flame-sealed them under vacuum in quartz ampules and observed their behavior upon melting. The salt composition was identical to that used in our previous work, but the scale was increased (total mass = 1.5 g) to better observe the system behavior. We begin with InAs NCs capped with GaI₃ ligands (Figure 1A) which are dispersed in a mixture of CsBr/KBr/LiBr and GaI₃ (Figure 1A). We observe that upon melting, the system phase segregates into a nearly colorless top phase and a darkly colored lower phase (some NCs stick to the wall of the ampule however closer examination shows the upper liquid phase is colorless). We elucidate that this salt composition is not a uniform system, and the InAs nanocrystals preferentially dissolve in the lower phase. This observation also holds for InAs capped with selenide ligands (Figure 1B), indicating generality with respect to nanocrystal surface chemistry. Further we observe the same behavior for a KI/LiI eutectic with added GaI3 and InAs nanocrystals capped with GaI₃ ligands (Figure 1C), indicating the halide identity does not qualitatively change the observation. We further observe identical behavior for InP nanocrystals and Pt nanocrystals (Figure S1) across a variety of salt compositions and surface chemistries, suggesting this behavior is endemic to these salt systems.

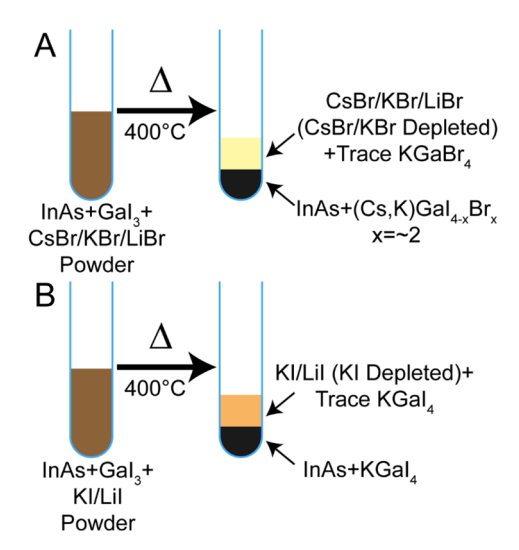
Spectroscopic Evaluation of Phase Separated Molten Salt Solvents. With the observation that colloidal nanocrystals segregate to one phase in molten mixtures of either GaI3 and the CsBr/KBr/LiBr eutectic, or mixtures of GaI3 and the KI/LiI eutectic, we aim to elucidate the chemical identity of this phase since it is likely crucial for the mechanistic understanding of colloidal chemistry in molten salts. We use a combination of in situ high-temperature UV-vis absorption spectroscopy and Raman spectroscopy to unambiguously identify the gallium halide moieties present in the molten salt phases observed. Raman spectroscopy enables us to precisely determine the chemical structure of the polyatomic gallium halide molecules and ions present in the salts, and UV-vis spectroscopy enables us to determine the relative concentrations of different species present. Compared with other analytical tools these two techniques together provide a wealth of insight and are relatively easy to implement for hightemperature in situ measurements. Other techniques to probe molten salt systems such as high-temperature NMR is limited by imprecise chemical specificity and difficult implementation at the temperatures relevant to this work. High temperature IR spectroscopy is limited by the overlap of the blackbody background with signal from the low frequency vibrational modes of interest.

We begin by preparing ampules with identical salt compositions as noted in Figure 1A-C without added nanocrystals. Indeed, we observe phase separation of the salt phases (Figure 1D-E, inset) without added nanocrystals and the phase separated layers adopt distinct colors. Extensive mixing, stirring, shaking, or heating (>550 °C) of the phase separated phases did not lead to homogenization. We use UVvis absorption spectroscopy to quantitively compare the observed color changes in our mixed phase systems with directly synthesized KGaI_xBr_{4-x} (x = 0-4) since this is a potential product due to the Lewis acid-base reaction between ABr (A = Li, K, Cs) species and GaI_3 . Due to the well-defined molecular structure of [GaX₄]⁻ species, the cation will have secondary effects on observed visible absorption spectra and Raman spectra compared to the halide identity. Later we will discuss how the alkali metal cations partition in these phaseseparated systems. In Figure 1D, we compare the UV–vis absorption spectrum of the molten lower phase at 450 °C resulting from the phase separated mixture of GaI₃ and the CsBr/KBr/LiBr eutectic (black trace) with absorption spectra from mixed halide potassium tetrahalogallate KGaI_xBr_{4-x} (x = 0-4) salts which are the likely product of the Lewis acid–base reaction between GaI₃ and CsBr/KBr/LiBr. For the mixed phase KGaI_xBr_{4-x} (x = 0-4), we observe a monotonic redshift of the absorption onset as x increases from 0 to 4. The absorption onset of the lower phase (black curve) corresponds well with the absorption onset for KGaBr₂I₂ suggesting that the lower phase consists of a mixed halide tetrahalogallate molten salt with $x \sim 2$.

We use room temperature Raman spectroscopy to better understand the structure and composition of the lower salt phase in the GaI₃ plus CsBr/KBr/LiBr mixture. The black trace in Figure 1F corresponds to the room temperature Raman spectrum from the solidified lower salt phase. We compare these to the directly synthesized KGaBr_{4-x} I_x (x = 0-4) salts (violet to green traces). The two parent compounds, KGaBr₄ and KGaI₄ show a single strong peak at ~210 and ~145 cm⁻¹ which correspond well with symmetric Ga-X stretch modes (v_1) for X = Br and X = I respectively. For the mixed halide KGaX₄ salts, we observe several additional Raman peaks appear. Two of the peaks match with parent KGaBr₄ and KGaI4 respectively. An additional 3 strong peaks appear as a series at frequencies higher than the [GaI₄] peak at ~145 cm⁻¹. These correspond to the Ga-I symmetric stretching from [GaI₃Br]⁻, [GaI₂Br₂]⁻, and [GaIBr₃]⁻ respectively. A similar series of 3 additional peaks arise at frequencies higher than the [GaBr₄] peak which correspond to the Ga-Br symmetric stretching from [GaIBr₃]⁻, [GaI₂Br₂]⁻, and [GaI₃Br]⁻, respectively. The Raman peak series observed here is analogous to the previously studied [GaBr_xCl_{4-x}] system, where the identity of the species was confirmed by Ga NMR.³¹ Together, the high-temperature UV-vis and Raman spectroscopy suggest that the lower phase which the nanocrystals phase separate to in the mixture of GaI3 and the CsBr/KBr/LiBr eutectic, consists of Lewis neutral mixed tetra bromo-iodo-gallate species (Scheme 2A).

Next, we turn our attention to the phase separated system consisting of GaI3 added to the KI/LiI eutectic. The hightemperature UV-vis spectra of the lower phase of the phase separated mixture (Figure 1E black curve) overlaps with directly synthesized KGaI4, suggesting that the lower phase consists of pure KGaI4. In addition, adding excess I in the form of KI does not change the absorption spectrum, suggesting that excess I does not change the speciation of KGaI₄. Room temperature Raman spectra of the above 3 samples (Figure 1G) show nearly identical spectra with a very strong peak at $\sim 145 \text{ cm}^{-1}$ which corresponds to the symmetric Ga-I stretch (v_1) and two weaker peaks at 77 and 58 cm⁻¹ which correspond to the asymmetric bend (v_4) and symmetric bend (v_2) for a tetrahedral molecule. These peaks are consistent with previous literature results.³² The Raman spectra thus strongly suggest that the lower phase of the molten salt mixture consists exclusively of [GaI₄] species. In addition, the near perfect overlap of the absorption spectra of KGaI₄ and the lower phase of the GaI₃ plus KI/LiI suggest that the lower phase consists entirely of [GaI₄]⁻ since any dilution would lead to a decreased absorbance. Scheme 2B shows our current understanding of the KI/LiI + GaI₃ reaction mixture. We note that a similar phase separation is observed for GaBr₃

Scheme 2. Schematic Depiction of the Outcome of Melting (A) CsBr/KBr/LiBr with Added Nanocrystals and Gallium Iodide and (B) KI/LiI with Added Nanocrystals and Gallium Iodide as Elucidated by the Spectroscopic Studies in This Work^a



"The ground powder of salt plus nanocrystals typically has a brown color before melting and a low density (large volume) due to empty space between powder particles (left). Upon melting (right), the density increases (volume decrease), and the phase separation becomes apparent due to the formation of two distinct layers. The black lower phase is indictive of colloidal InAs nanocrystals in a molten salt, and the lightly colored upper phase indicates no nanocrystals are present in that phase.

added to the CsBr/KBr/LiBr eutectic, indicating the halide identity is not responsible for the phase separation (Figure S2). Phase separation is observed in all cases where excess Lewis basic CsBr/KBr/LiBr is combined with InBr₃ or AlBr₃ (Figure S3A) and in cases where KI/LiI is combined with InI₃, or AlI₃ (Figure S3B). Based on these observations, it appears that a phase separation existed in our previously developed reaction conditions where we used excess Lewis basic components, ^{23,24} and the true reactive phases for molten salt mediated cation exchange were actually the Lewis neutral tetrahalogallate phases.

The prevalence of this phase separation across all gallium halide/alkali halide eutectic compositions suggests that halide identity is not responsible for these observations. Previous literature on the LiCl/KCl/AlCl₃ ternary phase diagram shows similar phase separations when there is an excess of LiCl and KCl relative to AlCl₃.³³ It was suggested that the small size of the Li⁺ cations relative to [AlCl₄]⁻ anions drives the system to preferentially phase separate into a KAlCl₄ phase and a LiCl/ KCl phase, rather than form a homogeneous solution.³³ Similarly here, Li⁺ is much smaller than the tetrahalogallate species, and thus, a similar driving force exists for phase separation. Another way to frame these observations is using hard soft acid base principles (HSAB), which were not wellestablished at the time of publication for ref 33. The Pearson Absolute Hardness (η) of Li^+ is 35.1 eV compared to 13.6 eV for K^+ and 10.6 eV for Cs^+ . Among Lewis bases, I^- has a very low hardness, $\eta \sim 3.7$ eV. $[GaI_4]^-$ ion can be even softer than I⁻, which indirectly follows from strong visible absorption of KGaI₄ (Figure 1E). According to the definition of Pearson

Absolute Hardness, $\eta = \frac{I-A}{2} \approx \frac{\varepsilon_{\text{LUMO}} - \varepsilon_{\text{HOMO}}}{2}$ where *I* and *A* are the ionization potential and electron affinity of any chemical system.³⁵ The visible absorption of [GaI₄]⁻ implies that the HOMO-LUMO gap of [GaI₄] is smaller than that of nearly colorless iodide molten salts. Correspondingly, $\varepsilon_{\text{LUMO}} - \varepsilon_{\text{HOMO}}$ and η of $[GaI_4]^-$ ions is smaller than that of iodide ions. [GaI₄] ion is much softer than Li explaining the driving force for [GaI₄]⁻ preferentially interacting with K⁺ compared to Li⁺. In support of this, high-resolution Raman shows slightly different frequencies for the symmetric Ga-I stretch from directly synthesized solid LiGaI4 compared to KGaI4 (Figure S4) enabling us to probe the counterion present in the lower phase. The Ga-I symmetric stretching frequency of the lower phase from a mixture of GaI₃ and the KI/LiI eutectic, matches well with pure KGaI₄ suggesting that potassium is primarily segregating to the lower phase (Figure S4). In addition, we observe that the upper phase solidifies at temperatures higher than the eutectic KI/LiI melting point suggesting the stoichiometry of the upper alkali halide eutectic has been altered, consistent with preferential segregation of the potassium to the lower phase. Altogether, the presence of Li⁺ containing salts in the low melting Lewis basic alkali halide eutectics used in our past reactions for gallium-based cation exchange universally led to phase separation of a AMX₄ species which the nanocrystals preferentially segregate to.

Synthesis of Colloidal $In_{1-x}Ga_xP$ and $In_{1-x}Ga_xAs$ Nanocrystals Using Lewis Neutral KGal₄ Molten Salts. Having identified KGaI₄ as the likely salt phase which the nanocrystals segregate to during molten salt annealing, we now use it directly to perform molten salt cation exchange reactions. We directly synthesize KGaI4 by comelting high-purity KI and GaI₃ in a quartz ampule, recovering it in an inert atmosphere glovebox, and grinding it into a coarse powder for use during cation exchange reactions. To perform a cation exchange reaction, the native organic ligands on colloidal InAs or InP nanocrystals are replaced with gallium iodide ligands via a biphasic ligand exchange. Here the nanocrystals with their native organic ligands in *n*-hexane (\sim 10 mL) are layered atop 5 mL of a 0.05 M solution of GaI₃ in anhydrous DMF and stirred until complete phase transfer of the nanocrystals to the DMF phase.²⁶ Inorganic ligand exchange is critical to remove all surface bound organic species which can decompose in the molten salts and deleteriously contaminate the molten salt reaction mixtures. Next the GaI3 capped InAs or InP nanocrystals are washed with acetonitrile to remove excess gallium iodide ligand, and dried as a powder in a glovebox. The dried nanocrystal powder is incorporated into finely ground KGaI4 in a mortar and pestle. The salt/nanocrystal mixture is loaded into an oven-dried (100 °C) quartz ampule, sealed under vacuum using an oxyhydrogen flame, and annealed at the desired temperature. We note that throughout this work we used flame-sealed quartz ampules since this provides a reliable and clean reaction environment. However, other more readily accessible reaction environments could be envisioned including using crucibles inside an inert gas tube furnace or open quartz tubes in a heating block or a muffle furnace inside an inert atmosphere glovebox. To recover the nanocrystals, the ampule is broken open in a nitrogen glovebox, the salt matrix dissolved using acetonitrile and the nanocrystals recovered as an insoluble powder by centrifugation. Finally, the nanocrystals were treated with a toluene solution of oleylamine to obtain a colloidal solution.

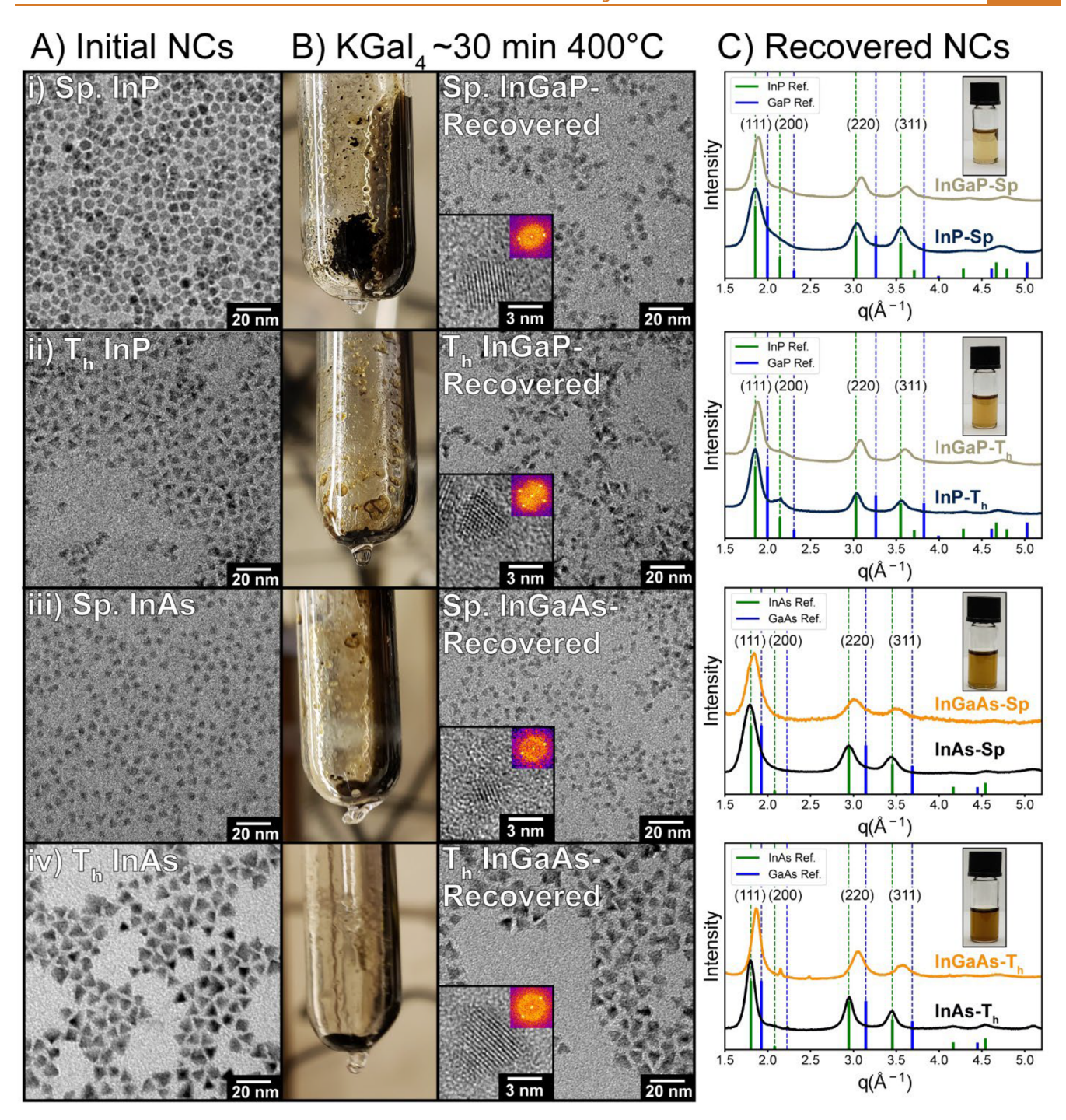


Figure 2. (A) TEM images of initial starting materials of (i) sphere-shaped InP nanocrystals, (ii) tetrahedron-shaped InP nanocrystals, (iii) sphere-shaped InAs nanocrystals, and (iv) tetrahedron-shaped InAs nanocrystals. (B) Photographs of a carefully tilted ampule showing material which has settled out of the molten salt phase and corresponding TEM images of the recovered nanocrystals. (C) Powder XRD patterns of the initial InP(As) nanocrystals and their corresponding $In_{1-x}Ga_xP(As)$ materials with inset photographs of colloidal solutions of the recovered nanocrystals.

In Figure 2, we show the results of several different colloidal III—V nanocrystals treated in molten KGaI $_4$ at 400 °C for 30 min. In Figure 2 column A, TEM images of initial III—V nanocrystals including (i) sphere-shaped InP nanocrystals, (ii) tetrahedron-shaped InP nanocrystals, (iii) sphere-shaped InAs nanocrystals, and (iv) tetrahedron-shaped InAs nanocrystals show well-separated individual nanocrystals typical of colloidal nanocrystals. Photos in Figure 2B show ampules of the molten salt/nanocrystal mixture at $T\sim400$ °C immediately after

removal from the furnace. The ampule has been rotated to reveal nanocrystal powders which have settled to the bottom of the ampule. This indicates either that the nanocrystals have imperfect colloidal stability in the KGaI₄ molten salt at elevated temperatures or the nanocrystal solubility in the molten KGaI₄ is lower than in other salt mixtures. Lowered colloidal stability in KGaI₄ would be consistent with the established molten salt colloidal stability principles, where Lewis neutral salt mixtures do not give long-term colloidal

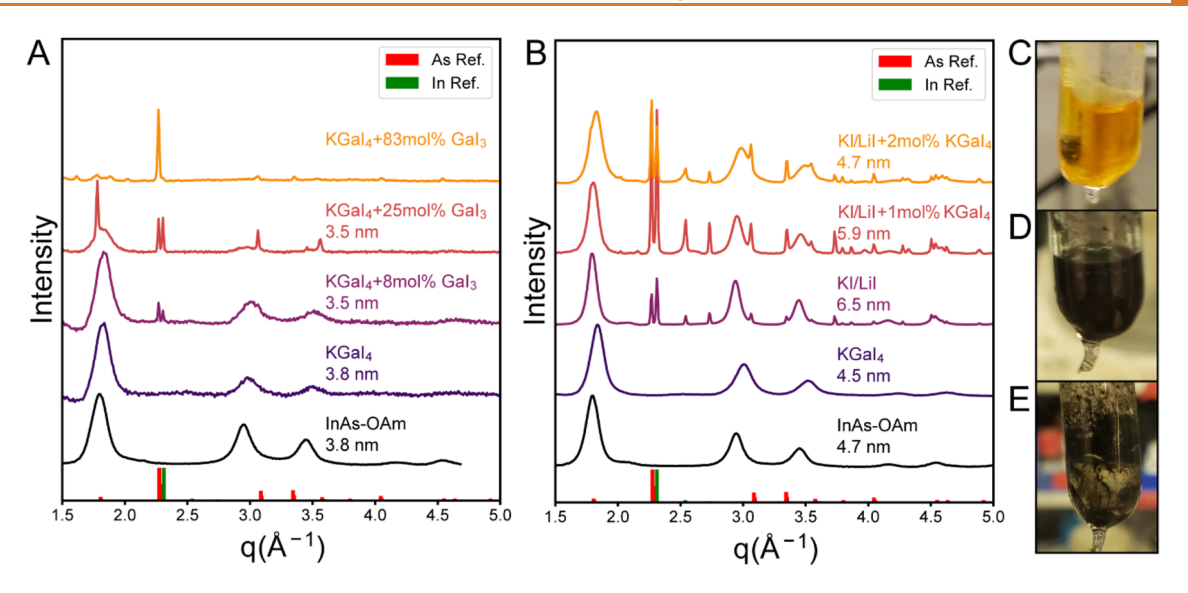


Figure 3. (A) Powder XRD patterns of the recovered products from annealing InAs nanocrystals in KGaI₄ at 400 °C for 30 min with added excess GaI₃. (B) Powder XRD patterns of recovered products from annealing InAs nanocrystals in KI/LiI eutectic at 400 °C for 30 min with small amounts of added KGaI₄. (C) Photo of 1 mol % KGaI₄ in KI/LiI eutectic with no added nanocrystals. Inside the ampule is a small tube which contains gallium metal (dark blob) to getter iodine vapor impurities in the sample without being in direct contact with the salt. (D) Photo of InAs nanocrystals dispersed in pure KI/LiI Eutectic at \sim 280 °C and (E) photo of the same ampule after adding KGaI₄ to make a 1 mol % solution in KI/LiI. Notice the colorless salt phase present in the photo in (E).

stability.²² The other possibility of limited solubility of nanocrystals in different molten salt solvents is equally probable, and while stability principles have been established, solubility limits of NCs in different salts have not. Despite this, we still recover high-quality colloidal nanocrystals as evidenced by well-separated individual nanocrystals by TEM (Figure 2B i-iv), stable colloidal solutions of oleylamine capped nanocrystals (Figure 2C i-iv, inset photo) in organic solvents, and small-angle X-ray scattering consistent with well-dispersed individual nanocrystals (Figure S5). This indicates the Lewis neutral salts still provide an effective barrier for nanocrystal fusion despite some settling out of the nanocrystal powders at high temperatures. Powder X-ray diffraction of the recovered InP and InAs nanocrystals (Figure 2C) show phase pure zinc blende diffraction peaks indicating there are no crystalline impurities in the samples. In addition, for samples of InP and InAs annealed in the KGaI4 molten salt, we observe shifts of the diffraction peaks to larger q (2θ) , indicating the lattice parameter of the nanocrystals has decreased, demonstrating that gallium has diffused into the lattice. Previous work from our group has shown that the PXRD peak shifts correspond to homogeneous alloying which was further confirmed by solidstate NMR;²⁵ however, for larger quantum dots in this work, a composition gradient cannot be ruled out. Further we observe nearly identical peak width for the KGaI₄ treated nanocrystals (light brown and orange lines, respectively) compared to the initial nanocrystals (black). Altogether, the alloyed $In_{1-x}Ga_xP$ and In_{1-x}Ga_xAs nanocrystals we recover after annealing in KGaI4 are very similar, in terms of gallium content and shape change as our previous results using Lewis basic molten salts with added gallium iodide.²⁴

The Lewis neutral reaction conditions afforded by the KGaI₄ molten salt solvent provide chemical stability of III–V phases at high temperatures. We explored the reactivity of InAs nanocrystals in KGaI₄ up to 650 $^{\circ}$ C, and we can recover phase pure GaAs powders (Figure S6A). However, we see that the Scherrer size of the nanocrystals begin to increase at ~450 $^{\circ}$ C.

For samples annealed at 650 °C, the Scherrer size has increased to ~50 nm and TEM (Figure S7A) corroborates the size increase. We explored using Se-capped InAs nanocrystals at elevated temperatures in the KGaI4 molten salt and found similar chemical stability of the InAs nanocrystals up to 650 °C (Figure S6C). Interestingly, for InAs nanocrystals capped with selenide ligands, the Scherrer size did not increase as dramatically compared to GaI3-capped nanocrystals. The domain size began to increase at ~550 °C (Figure S6D), and samples treated at 650 °C grew to ~20 nm Scherrer sizes. TEM shows particle sizes that are consistent with the XRD results (Figure S7B). These results demonstrate that the Lewis neutral molten salt environment provides a chemically benign reaction condition to process III-V nanocrystals, and that molten salts are viable solvents for III-V materials for temperatures as high as 600 °C. We found InP nanocrystals were less thermally stable than InAs nanocrystals during hightemperature annealing in KGaI4. For example, when heated to temperatures up to 450 °C, we observe the formation of In_{1-x}Ga_xP nanocrystals, but at temperatures higher than 450 °C we observe decomposition of the InP. In the case of III–P materials, thermal stability is decreased due to the high vapor pressure of phosphorus compared to III-As materials.

Accelerated Decomposition Observed in Reactive Lewis Acidic and Lewis Basic Molten Salt Solvents. Having established that Lewis neutral molten salt phases are the phase that likely formed in our previous works, we aim to carefully modify the salt composition to understand how excess acidic or basic components affect III—V nanocrystals. For the KI/GaI₃ phase diagram in the >50% mole fraction GaI₃ region, the system forms a homogeneous melt across all compositions if the salt is above the melting point of KGaI₄ and GaI₃. Figure 3A shows the results of annealing InAs nanocrystals at 400 °C for 1 h in increasingly Lewis acidic GaI₃/KI molten salt. As the amount of excess GaI₃ is increased, we observe an increase in the amount of decomposition products (In⁰ and As⁰) and a decrease in diffraction intensity from the expected zinc blende

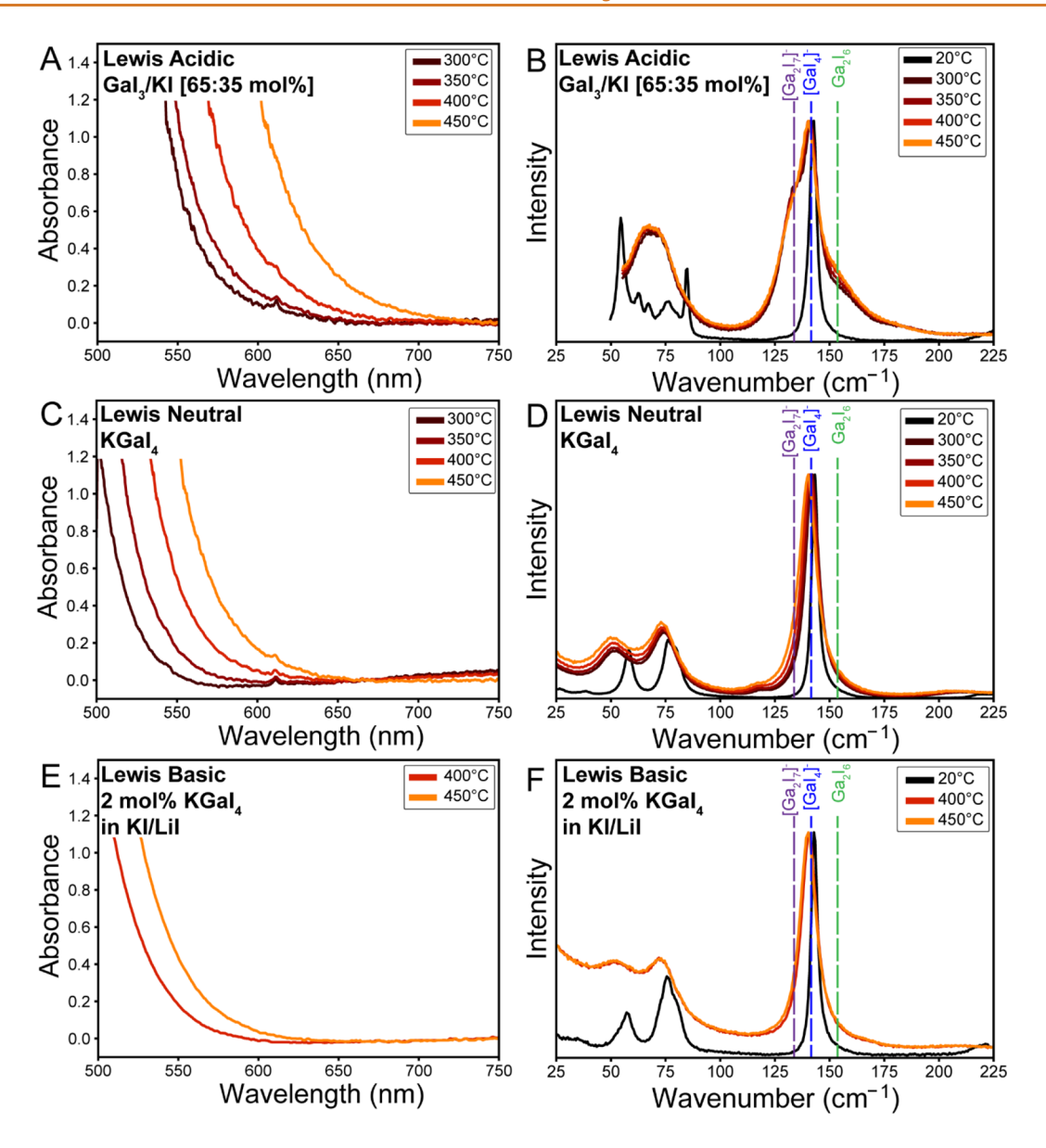


Figure 4. In situ high-temperature spectroscopy of molten salt solvents. Visible absorption spectra and Raman spectra for (A, B) the nominally Lewis acidic GaI_3/KI [65:35 mol %] eutectic mixture, (C, D) the nominally neutral $KGaI_4$ and (E, F) the nominally Lewis basic 2 mol % $KGaI_4$ in KI/LiI eutectic. The violet, blue, and green lines correspond to the expected Ga-I stretching frequencies unique to $[Ga_2I_7]^-$, $[GaI_4]^-$, and Ga_2I_6 respectively.

peaks of $In_{1-x}Ga_xAs$ to the point where no detectable $In_{1-x}Ga_xAs$ is recovered. Our results indicate that InAs is susceptible to decomposition in the presence of excess acidic salt components. Interestingly our previous work using Lewis acidic molten salts for preparation of $In_{1-x}Ga_xP$ nanocrystals from InP did not suffer from decomposition in the same GaI_3/KI [65:35 molten salts], indicating that the chemical identity of the nanocrystals also plays a role in determining chemical stability.

Next, we explore the chemical and colloidal stability of InAs nanocrystals in truly Lewis basic environments rather than in salt systems where phase separation occurs. Due to the phase separation of $KGaI_4$ with excess KI/LiI, care must be taken to engineer a single-phase gallium containing molten salt environment. The upper KI/LiI phase from separated mixtures (inset photo Figure 1E) is also colored, indicating that some $\left[GaI_4\right]^-$ is present in the upper salt phase. We find that we can

add up to 2 mol % (~10 wt %) KGaI₄ to a KI/LiI eutectic mixture without obvious phase separation (Figure 3C) when no nanocrystals are present. Interestingly, we find that InAs nanocrystals form well dispersed colloids in pure KI/LiI eutectic mixture (Figure 3D) but upon addition of even 1 mol % KGaI4 the nanocrystals appear to lose solubility in the Lewis basic molten salt mixture (Figure 3E). This indicates that even small amounts of [GaI₄] can lead to precipitation of the nanocrystals from the KI/LiI salt matrix. One possibility is that the additional gallium halide species change the nanocrystal surface chemistry, such that a charge density wave is no longer seeded by the charged nanocrystal surface.²⁷ A second possibility is that nanocrystals can be thought of as very large cations, and similar to the driving force leading to phase separation of KI/LiI+GaI3 mixtures, nanocrystals would preferentially interact with the large [GaI₄] anions in KGaI₄, and thus, the two components phase separate into a

highly concentrated nanocrystal/KGaI $_4$ phase and a nanocrystal and KGaI $_4$ deficient phase. Regardless of origin, one way to frame this observation is an example of a "flocculant" or "antisolvent" for molten salt colloids which we believe is the an example of many possible ways of controlling nanocrystal solubility using salt additives.

Annealing InAs nanocrystals in the pure KI/LiI eutectic at 400 °C (Figure 3B) leads to formation of As⁰ and In⁰ decomposition products. Further the InAs nanocrystal grow larger than nanocrystals treated in KGaI₄ as seen by the change in peak width. This indicates the excess Lewis base components of the salt may facilitate mass transfer between nanocrystals. For example, if the reaction InAs+3NaI→ Na₃As + InI₃ occurs to a small extent, the products can effectively shuttle InAs units between nanocrystals, or can undergo direct redox to form As⁰ and In⁰. Further, upon addition of solvents during the recovery process, Na₃As and InI₃ can undergo redox reaction to decompose into As⁰ and In⁰ respectively. Addition of 1-2 mol % (5-10 wt %) KGaI₄ to the KI/LiI molten salt containing InAs nanocrystals followed by annealing at 400 °C (Figure 3B) leads to incorporation of gallium as evidenced by shift of the X-ray diffraction peaks to higher q-values. However, we also observe significant decomposition products in the form of indium metal and arsenic. In these reactions, the nanocrystals likely have segregated to a very small KGaI4 phase, but they may also be in contact with pure KI/LiI phase leading to enhanced decomposition.

The phase separation of molten salts is typically driven by large differences in ionic radii, with Li⁺ being an example of a small cation phase-separating from other ions. Therefore, we further explored using a CsI/NaI/KI eutectic which melts at ~410 °C and importantly does not contain Li⁺. ³⁶ We find that this salt composition can dissolve GaI₃ up to 10 mol % (50 wt %) without phase separation (Figure S8A). We explored using the CsI/NaI/KI salt for molten salt processing of InAs nanocrystals capped with GaI₃ ligands and found the nanocrystals were destroyed after annealing at 450 °C (Figure S8B). We further found that Se-capped InAs had improved chemical stability both with and without added KGaI4; however the reactions suffered from low yield, unidentified byproducts, and irregular XRD peak shapes. One issue with this molten salt mixture is the high melting point, and it is possible that heating the InAs nanocrystals to T > 400 °C before the salt melts may explain the enhanced decomposition we observe in these salts. In all, we have explored a few deviations from the neutral KGaI4 molten salt mixture and found that excess Lewis acidic or Lewis basic components can lead to accelerated decomposition of sensitive InAs nanocrystals. While these observations provide guidance, we are careful to emphasize that different materials systems may have different reactivity to a given molten salt environment.

In Situ Spectroscopy to Evaluate Chemical Species Present in Molten Salts at Elevated Temperatures. Given that the molten salt reactions occur at elevated temperatures, the chemical species identified by room-temperature spectroscopy may not be representative of the species present at the reaction temperature. Qualitatively we observe that increasing the temperature of molten KGaI₄ causes the sample to develop an increasingly deep red color (Figure S9A). Further, we observe that increasing the GaI₃-to-KI ratio causes the red color to develop more intense (Figure S9B), suggesting temperature may be changing the chemical species present in the molten salt phases.

ı

We perform temperature-dependent visible absorption spectroscopy and Raman spectroscopy on the molten salts used in this work to elucidate changes in chemical species present as a function of temperature. Figure 4A shows temperature-dependent absorption spectra of the GaI₃/KI [65:35 mol %] eutectic mixture which shows a progressive redshift of the absorption onset as the temperature increases from 300 to 450 °C. This is consistent with either temperature-dependent speciation of components with different absorption spectra or drastic change in the temperature-dependent absorption spectra of the GaI₃/KI [65:35 mol %] eutectic salt. Unfortunately, due to the strong extinction and likely broad absorption features of the salt components at these elevated temperatures, we do not observe distinct peaks or an isosbestic point for further quantitative analysis.

At room temperature, the GaI_3/KI [65:35 mol %] eutectic salt shows 5 Raman peaks in the $50-100~cm^{-1}$ range and a very strong peak at $\sim 142~cm^{-1}$ (Figure 4B Black). To understand the origin of these peaks, we compare the room-temperature Raman spectra for GaI_3 , $KGaI_4$, and the GaI_3/KI [65:35 mol %] eutectic mixture (Figure S10). The Raman spectrum of the KI/GaI_3 eutectic appears to be a mixture spectrum of GaI_3 and $KGaI_4$ where the peaks at 55, 62, 67, and 84 cm⁻¹ correspond to GaI_3 and the peak at 76 cm⁻¹ corresponds to $KGaI_4$, indicating that at room temperature the salt contains a mixture of $[GaI_4]^-$ anions and Ga_2I_6 . This is different than what is seen for the GaI_3/CsI and GaI_3/RbI systems where Cs^+ $[Ga_2I_7]^-$ and Rb^+ $[Ga_2I_7]^-$ form³⁷ and likely the smaller size of the K^+ ion plays a role in the observed difference.

At elevated temperatures, the Raman spectra of the GaI₃/KI [65:35 mol %] eutectic show 2 broad features at ~70 and ~140 cm⁻¹ where the peak at 140 cm⁻¹ likely consists of at least three overlapping peaks. We suggest that the three overlapping peaks at 140 cm⁻¹ correspond to three different species which are expected to be present in the Lewis acidic GaI₃/KI [65:35 mol %] eutectic salt. The first shoulder at ~137 cm⁻¹ likely corresponds to $[Ga_2I_7]^- v_s$ and v_{as} modes which are strongly Raman active.³⁷ Overlapping with that peak is the peak at ~ 145 cm⁻¹ which corresponds to the v_1 (symmetric stretch) mode of [GaI₄]⁻. Free Ga₂I₆ also has a strong Raman mode at ~147 cm⁻¹; thus, the presence of the peak at ~145 cm⁻¹ is consistent with both species being present. The identity of the shoulder which we observe at \sim 153 cm⁻¹ is difficult to assign and has not been reported to our knowledge. However, we note that reported experimental spectra of molten Ga₂I₆ show a distinct shoulder on the highfrequency side of the main peak at $\sim 143~\text{cm}^{-1.38}$ We also observe the same high frequency shoulder at ~153 cm⁻¹ for pure molten gallium iodide (Figure S11B), strongly suggesting that the shoulder peak at ~ 153 cm⁻¹ is indicative of a Ga₂I₆ species present in the GaI₃/KI [65:35 mol %] molten salt eutectic. Further, we do not observe a shoulder at ~ 153 cm⁻¹ for KGaI4 or KGaI4 in KI/LiI, compositions which should not contain any free Ga₂I₆, consistent with our assignment of the shoulder at ~153 cm⁻¹ being attributed to a Ga₂I₆ species. Based on these spectroscopic observations, it appears that at room temperature, the GaI₃/KI [65:35 mol %] eutectic salt primarily contains [GaI₄]⁻ and Ga₂I₆ however upon melting the mixture of chemical species becomes more complex, now containing a mixture of [GaI₄]⁻, [Ga₂I₇]⁻, and Ga₂I₆. Our results suggest that at elevated temperatures significant Ga₂I₆ and $[Ga_2I_7]^-$ is present in the molten salt.

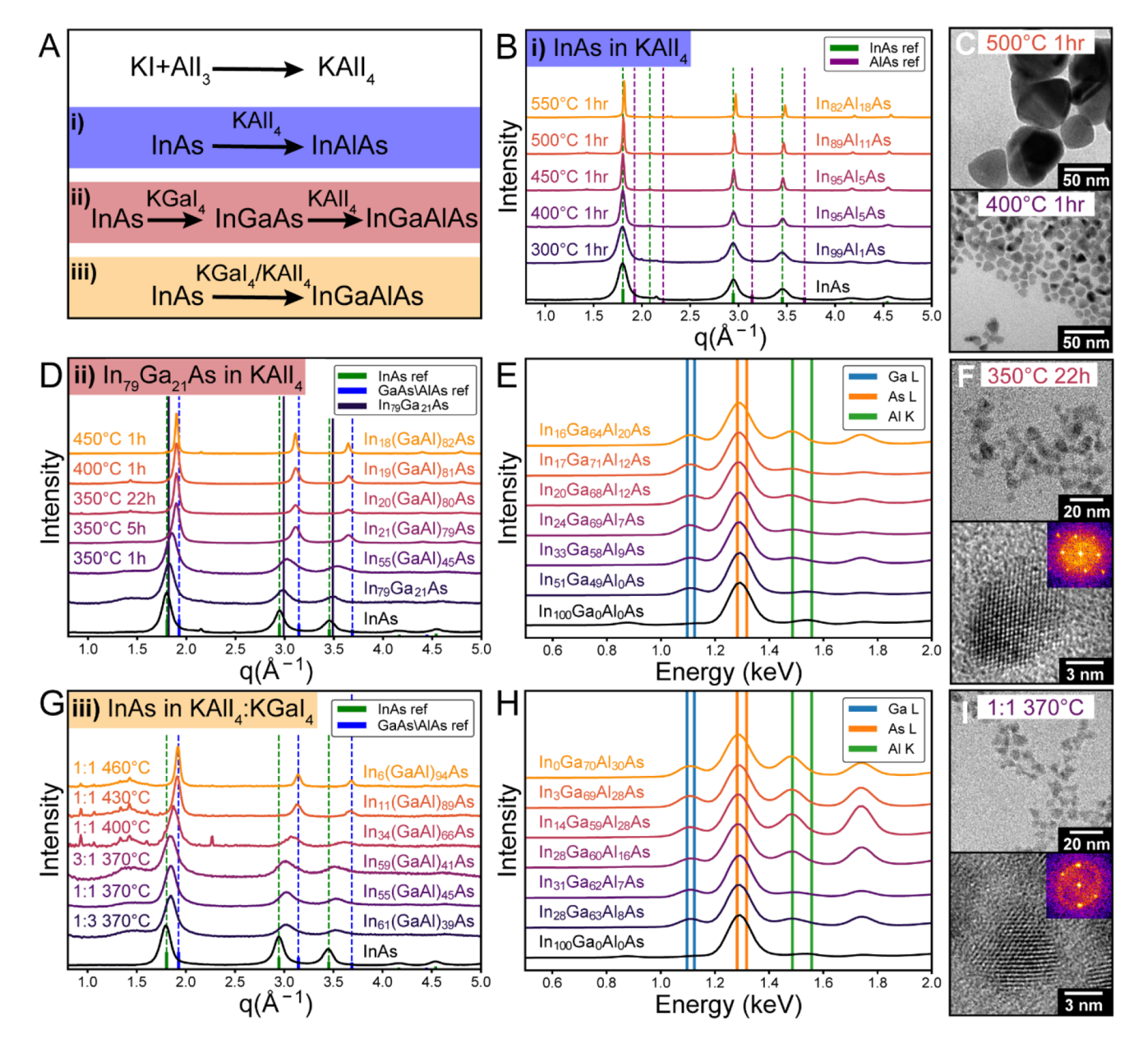


Figure 5. (A) Reaction schemes using KAlI₄ for preparing (i) $In_{1-y}Al_yAs$, (ii) $In_{1-x-y}Ga_xAl_yAs$ via a two-step reaction, and (iii) $In_{1-x-y}Ga_xAl_yAs$ via a single-step reaction. (B) Powder XRD patterns for InAs nanocrystals after annealing in KAlI₄ under different conditions and (C) corresponding TEM images for a subset of the samples. (D) XRD patterns for $In_{79}Ga_{21}As$ annealed in KAlI₄ under different conditions with their corresponding composition determined by Vegard's law as discussed in the text, (E) XRF spectra of the same samples with their corresponding composition quantification, and (F) TEM and HRTEM for a subset of the samples. (G) XRD patterns for InAs annealed in KAlI₄/KGaI₄ under different conditions with their corresponding composition determined by Vegard's law as discussed in the text, (H) XRF spectra of the same samples with their corresponding composition quantification, and (I) TEM and HRTEM for a subset of the samples.

For the KGaI₄, we observe progressive redshift of the absorption onset as the temperature is increased (Figure 4C), consistent either with different chemical species forming or simply temperature-dependent absorption spectrum changes for the $[GaI_4]^-$ anion. Room-temperature Raman spectra of KGaI₄ (Figure 4D) show three well-defined peaks at 146, 80, and 60 cm⁻¹ corresponding to the v_1 (symmetric stretch), v_4 (asymmetric bend), and v_2 (symmetric bend) respectively for a tetrahedral molecule.³⁹ Temperature-dependent Raman spectra show that three distinct peaks corresponding to the v_1 , v_4 and v_2 at 143, 75, and 50 cm⁻¹ remain. We observe a small

peak at $\sim 115~\text{cm}^{-1}$ which may correspond to small amounts of the $[Ga_2I_6]^{2-}$ ion which could form if a small amount of metallic gallium impurities were present in the system. Importantly we do not see any peaks or shoulders which correspond to Lewis acidic species such as GaI_3 or the $[Ga_2I_7]^-$ ion. Directly overlaying the Raman spectra for $KGaI_4$ and $KGaI_4$ in contact with excess AI $(A = Li_1K)$ shows no discernible difference (Figure S12) indicating $2KGaI_4 \rightarrow KI + KGa_2I_7$ does not happen to an appreciable amount. Further, the well-defined Raman peaks of $KGaI_4$ at elevated temperatures indicate that the molecular structure of this salt remains

as a well-defined $[GaI_4]^-$ molecular unit. Based on these observations, the neutral $KGaI_4$ molten salt remains primarily in the Lewis neutral $[GaI_4]^-$ state at elevated temperatures, and this provides a chemical basis to understand which molten salt solvents will prevent decomposition of colloidal nanocrystals.

Next, we turn our attention to the properties of dilute KGaI₄ dissolved in the KI/LiI eutectic (Figure 4E,F) to understand if the presence of excess I will modify the structure and thus reactivity of the gallium halide species. High-temperature visible absorption spectroscopy (Figure 4E) shows that the absorption onset occurs at shorter wavelengths than the corresponding pure KGaI4 at a given temperature, consistent with dilution of the KGaI₄ in a colorless KI/LiI matrix. Roomtemperature and high-temperature Raman spectra show the three distinct peaks corresponding to the v_1 , v_4 and v_2 at 143, 75, and 50 cm⁻¹, respectively, for the [GaI₄] molecule. We do not observe other peaks, indicating that in an iodide rich environment the primary gallium halide species present is [GaI₄]. Importantly these observations show that the enhanced decomposition in Lewis basic salt mixtures (Figure 3B) is likely a result of the implied excess I (which has no vibrational signatures) rather than the formation of a different gallium iodide species in the iodide rich environment.

Toward Aluminum Pnictide Alloy Colloidal Nanocrystals Using KAll₄ Molten Salts. Aluminum trihalides are the strongest Lewis acids of the group III halides. Previous attempts in our group to use aluminum halide molten salts to prepare aluminum pnictide phases resulted in complete decomposition of the colloidal nanocrystals. Here we decrease the reactivity of aluminum iodide (already the least reactive of the aluminum halides) by preparing the Lewis neutral form KAlI₄ from AlI₃ and KI (Figure 5A). We note that commercial sources of AlI₃ are often contaminated with iodine impurities which had to be removed via appropriate purification (Figure \$13). First, we explore reacting InAs nanocrystals, which we initially capped with AlI₃ ligands, with pure KAlI₄ (Figure 5Ai) to prepare $In_{1-x}Al_xAs$ nanocrystals. Annealing InAs at 300 °C for 1 h did not result in incorporation of Al (Figure 5B), and the nanocrystal Scherrer size did not change. Importantly, though, recovery of the InAs after high-temperature annealing indicates that creating a Lewis neutral KAlI₄ molten salt afforded chemical stability of the InAs phase. Highertemperature annealing (400-450 °C) resulted in ~5% Al incorporation accompanied by an increase in crystallite size, but importantly the materials remain as well-separated nanocrystals (Figure 5C). At temperatures above 500 °C, 11–15% Al incorporation is observed, but the size increases dramatically. The sharp diffraction peaks indicate large crystallite domains and TEM shows the particles are now larger than 100 nm and contain multiple domains as evidenced by varying diffraction contrast within individual particles (Figure S14). Our results thus indicate that for InAs, the nanocrystals begin to ripen significantly at temperatures below the critical temperature needed to activate aluminum interdiffusion processes. We also explored Se-capped InAs nanocrystals, which we previously found increased the threshold temperature for ripening in the InAs-KGaI₄ system (Figures S6). We found that Se-capped InAs would decompose upon exposure to KAlI₄ molten salts (Figure S15). Our experiments show neutral KAII₄ molten salts afford chemical stability to III-V nanocrystals in Al-containing molten salts

which may enable future molten salt mediated growth of wide band gap Al-containing shell materials.

Next, we explore a two-step approach to prepare In_{1-x-y}Ga_xAl_yAs nanocrystals by first preparing In_{1-x}Ga_xAs nanocrystals by annealing InAs nanocrystals in KGaI4 followed by annealing the $In_{1-x}Ga_xAs$ nanocrystals in KAlI₄. This approach is motivated by the observation that In_{1-x}Ga_xAs nanocrystals show higher resilience toward etching or growth in molten salts compared to InAs nanocrystals. Figure 5D shows powder X-ray diffraction patterns for initial InAs nanocrystals (black) and after gallium incorporation (dark violet) indicating the nanocrystals have ~21% gallium incorporated. Next these nanocrystals are recovered from the KGaI₄ molten salt by dissolving the salt matrix in acetonitrile and separating the nanocrystal powder by centrifugation. The powder was subsequently dried a second time, incorporated in the KAlI₄ salt using a mortar and pestle, and annealed at high temperatures in sealed quartz ampules. Nanocrystals were recovered as colloidal solutions via an approach similar to KGaI4 reactions, except that MeCN was replaced with a mixture of MeCN and DMF to better dissolve the KAlI₄.

Powder X-ray diffraction of the recovered In₆₉Ga₂₁As nanocrystals after KAlI₄ treatment (Figure 5D) shows broad peaks consistent with small crystallite size, with peaks getting slightly sharper for higher-temperature annealing. In addition, we observe continued shifting of the XRD peak positions to larger q-values with increased time and temperature. AlAs and GaAs have nearly identical lattice parameters; thus, the observation of shifted diffraction peaks is consistent with either Al or Ga incorporation into the InAs lattice. We estimate the In:(Ga+Al) ratio based on a linear interpolation of the InAs and GaAs/AlAs lattice parameters. Based on this analysis framework, we observe higher-temperature annealing leads to more (Al+Ga) incorporated into the lattice. In Figure 5E, Xray fluorescence is used to independently determine the amount of indium, gallium, and aluminum in the nanocrystals. We observe more gallium has been incorporated into the nanocrystals than the initial 21% from the KGaI₄ pretreatment, and at most we have incorporated 20% Al for 450 °C annealing temperatures. We suspect the gallium content increase is a result of partial nanocrystal decomposition, where some of the initial In_{1-x}Ga_xAs nanocrystals decompose providing an additional source of gallium for cation exchange. Further these results suggest preferential uptake of Ga into the nanocrystals over Al considering the much higher concentration of Al over the Ga (from particle decomposition) in the salt. TEM images of the recovered $In_{1-x-y}Ga_xAl_yAs$ nanocrystals (Figure 5F) show small crystallite sizes and single crystal domains by HRTEM. Using this approach with In_{1-x}Ga_xAs nanocrystals which initially contain 55% Ga (Figure S16) yielded similar trends but with overall less Al incorporation. Altogether our results show that a two-step molten salt annealing approach is a viable route to quaternary $In_{1-x-v}Ga_xAl_vAs$ nanocrystals.

Next, we explore the reactivity of InAs nanocrystals which we anneal in a mixture of KAlI₄ and KGaI₄ in a single step (Figure 5A-iii). The idea here is that we can "temper" the reactivity of Al-halide molten salts by diluting them with Gahalide salts. For all reaction conditions, we observe shifts of the diffraction peaks to larger q-values indicating incorporation of Ga and/or Al into the lattice (Figure 5G), and XRF (Figure 5H) is used to discern the exact compositions of In, Ga, and Al, respectively. First, we discuss the effect of the ratio of

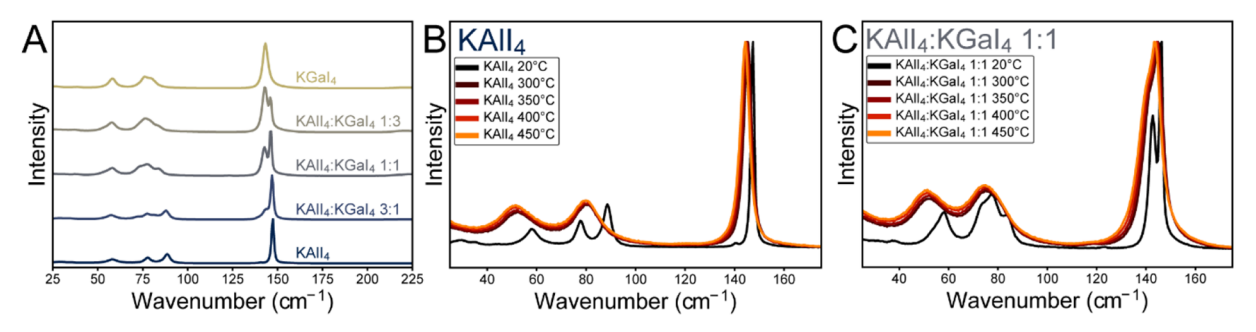


Figure 6. (A) Room-temperature Raman spectra of mixed $KGaI_4$ and $KAII_4$ which were previously fused at \sim 400 °C prior to solidification. (B) High-temperature Raman spectra of KAII₄. (C) High-temperature Raman spectra of molten mixture of $KGaI_4$ and $KAII_4$ with a 1:1 molar ratio.

KAlI₄:KGaI₄ annealed at 370 °C for 1 h, and we find that with larger amounts of KAlI₄ there is an increase in the Al content of the nanocrystals. In addition, we see that there is preferential incorporation of Ga over Al despite the large excess of Al, consistent with our observations for the two step reactions. Importantly the peak widths do not appreciably broaden when annealed at 370 °C indicating we can control the size of the particles while still incorporating Al into the lattice. Next, we explore the role of temperature from 370 to 460 °C for a 1:1 ratio of KAlI4:KGaI4. Here we observe that at higher temperatures, the powder diffraction peaks progressively shift to higher q-values indicating more Ga+Al has been incorporated into the lattice. Further, we observe that at higher temperatures the diffraction peaks become sharper, indicating the particles begin to grow at temperatures above 400 °C. X-ray fluorescence shows that increasing the temperature causes more indium to be expelled out of the lattice and that for temperatures greater than 400 °C, ~30% Al can be incorporated with all indium removed, resulting in Ga₇₀Al₃₀As nanocrystals. Importantly, TEM imaging shows that the particles derived from mixed gallium/aluminum salts show better defined shapes (Figure 5I). Qualitatively the mixed salt reactions had higher yields and better colloidal stability after recovery compared to the reactions involving pure KAlI₄. Altogether the mixed salt approach appears to temper the high reactivity of pure KAlI₄.

We expand the mixed salt approach using mixed KAlI₄:KInI₄ in attempts to prepare pure ${\rm In}_{1-x}{\rm Al}_x{\rm As}$ while maintaining small nanocrystal sizes. Unfortunately, we found that mixed In/Al salts did not result in aluminum incorporation into InAs after annealing at 500 °C for 1 h in KAlI₄ containing 25% and 50% KInI₄ (Figure S17). Further we found that in high indium content salts (66% KInI₄), the particles decomposed significantly, and we were unable to identify any crystalline decomposition products. These observations suggest that the nature of indium-containing molten salts may be different than their gallium counterparts with regards to chemical stability and is consistent with previous attempts in our lab to use indium halide molten salt solvents.

Expanding mixed $KGaI_4/KAII_4$ salt approach to InP nanocrystals resulted in mixed $In_{1-x-y}Ga_xAI_yP$ nanocrystals (Figure S18). The material showed well-defined zinc blende diffraction peaks which do not broaden compared to the parent InP nanocrystals, indicating the particles did not change size. We measure up to 11% Al incorporation into the phosphide lattice based on X-ray fluorescence. TEM (Figure S18C) shows the particles remain well dispersed and contain single crystal domains. Interestingly, we see that using a two-

step approach where we anneal $In_{1-x}Ga_xP$ nanocrystals in KAII₄ (Figure S18D) does not result in measurable aluminum incorporation and we also see significant decomposition of the particles indicating the mixed salt environment may provide enhanced stability. While the 11% Al incorporation is modest, the ability to disperse phosphide-based III–V nanocrystals in Al containing molten salts may enable future growth of wide band gap Al-containing shells using molten salts.

Understanding the Structure of Mixed KAll₄/KGal₄ Molten Salt Environments Using In Situ Raman Spectroscopy. One interesting trend we observe is that exposure of InAs and In_{1-x}Ga_xAs nanocrystals to pure KAlI₄ results in more particle growth than exposing the nanocrystals to mixed KAlI₄/KGaI₄ molten salts for nearly identical reaction conditions. We aim to elucidate a chemical explanation for the observed trends. Figure 6A shows room-temperature Raman spectra of mixed KAlI₄/KGaI₄ molten salts. For KAlI₄, at room temperature we observe a very strong peak at ~148 cm⁻¹ which corresponds to the symmetric stretching (v_1) mode of the [AlI₄] ion. We see a similar mode for the [GaI₄] anion at 145 cm⁻¹ which is broader than the $[AlI_4]^-$ ion. When mixed, we observe a linear combination of the $[AlI_4]^-$ and [GaI₄] spectra indicating more complex species do not form at room temperature. The low frequency Raman features of the KAlI₄ and KGaI₄ in the 50–100 cm⁻¹ range also show a linear combination of the two parent compounds. Based on this, mixed KAlI₄/KGaI₄ salts remain as distinct molecular units at room temperature.

At high temperatures, the Raman spectra of molten KAlI₄ retains the very strong peak at 148 cm⁻¹, and we observe small shifts to lower frequencies as the temperature is increased (Figure 6B). In addition, we observe that the two peaks at \sim 75 and ~90 cm⁻¹ observed in the solid state become one peak in the molten state. In the solid state KAlI₄ likely adopts a crystal structure which has multiple Al-I bond lengths leading to a Raman spectrum which differs from an ideal tetrahedral molecule. 41,42 Upon melting, the environment surrounding the [AlI₄] anions becomes more symmetric on average leading to the recovery of a Raman spectrum for an ideal tetrahedral molecule. The Raman peaks we observe are in good agreement with previous literature reports for Raman spectra of molten CsAlI₄⁴³ and demonstrate that the well-defined molecular structure of the [AlI₄] unit is maintained at the reaction temperatures.

Next, we turn our attention to the mixed $KAII_4/KGaI_4$ system where we observe a distinct color change for the mixed salts compared to their parent compounds (Figure S19) in the molten state. Room-temperature Raman spectra for a 50:50

mol % mixture of KAlI₄/KGaI₄ show a Raman spectrum that is a linear combination of the parent compounds (Figure 6C). Upon melting, we observe a broad asymmetric peak which we suspect is the overlapping symmetric stretch peak coming from the $[AlI_4]^-$ at ~ 144 cm⁻¹ and $[GaI_4]^-$ at ~ 140 cm⁻¹. Due to the broad and overlapping nature of the low frequency (50-100 cm⁻¹) peaks for KAlI₄ and KGaI₄ at room temperature, at elevated temperature these peaks devolve into 2 broad peaks. Based on the Raman data presented here it appears that the mixed KAlI₄ and KGaI₄ remain as their distinct [AlI₄] and [GaI₄] structural units in the molten state. As such it appears that our observation of the tempered reactivity of KAlI₄ when mixed with KGaI4 is a result of an effective dilution of the more reactive Al-salt in the less reactive Ga salt rather than the formation of distinct mixed Al-Ga molecular species. Two additional possibilities related to the materials' stability are also possible. First, we have empirically observed GaAs is more stable than InAs during molten salt annealing, and as such the addition of gallium into the nanocrystals increases their stability and thus mitigates decomposition in the Al-containing salts. Second, the excess gallium present in the system could prevent decomposition of the nanocrystals by forcing any decomposition products to immediately convert back to GaAs units which are more stable than AlAs units. Altogether, the distinct reactivity of mixed composition molten salt solvents toward nanocrystals demonstrates many routes to transform colloidal nanocrystals into ever more complex structures with compositions which are not accessible in organic solvent-based synthesis.

CONCLUSIONS

In this work, we have extensively explored the reactivity of molten salt solvents toward colloidal III-V nanocrystals, with a particular focus on the more sensitive III-arsenides, with regards to chemical and colloidal stability. We identify that many previously developed molten salt mixtures used for cation exchange underwent an unexpected phase separation due to the presence of small Li⁺ cations relative to the larger tetrahalogallate species. Fortuitously this resulted in a Lewis neutral salt environment which we found was key to preserving chemical stability of sensitive InAs nanocrystals. In addition, we demonstrate that directly prepared KGaI4 molten salts are excellent solvents for cation exchange of colloidal nanocrystals and that well-defined colloidal nanocrystals with precisely faceted shapes can be produced in these molten salts. Through in situ high-temperature Raman spectroscopy we demonstrate that the Lewis neutral molten salts based on alkali tetrahalogallate species retain the well-defined [MX₄] unit at the reaction temperature. We further explore using Lewis neutral KAlI₄ molten salts to prepare Al-based III-V alloys, demonstrating examples of colloidal In_{1-x-v}Ga_xAl_vAs and Ga_{1-x}Al_xAs nanocrystals through a variety of strategies to temper the reactivity of aluminum halide based molten salts toward sensitive III-V nanocrystals. Altogether our results show several key factors which must be considered when designing molten salt solvents for cation exchange of III-V nanocrystals.

METHODS

Chemicals. Trioctylphosphine (TOP, 97%), trioctylphosphine oxide (TOPO, 99%), diisobutylaluminum hydride (reagent grade, 1 M solution in toluene) and anhydrous solvents (hexane, toluene, ethanol (EtOH), isopropanol (IPA), acetonitrile (MeCN), methyl

acetate) were purchased from Sigma-Aldrich and used as received. Oleylamine (OAm, technical grade, 70%) and Oleic acid (OA, 90%) were purchased from Sigma-Aldrich and degassed under dynamic vacuum at 110 °C for several hours before storage in a nitrogen glovebox. Potassium iodide (ultradry, 99.998%), gallium(iii) iodide (ultradry, 99.999%), aluminum(iii) iodide (ultradry, 99.999%), lithium iodide (ultradry, 99.98%), sodium iodide, (ultradry, 99.98%), cesium iodide (ultradry, 99.98%), cesium bromide (ultradry, 99.9%), lithium bromide (ultradry, 99.9%), potassium bromide (ultradry, 99.9%), indium(i) chloride (99.995%) and N,N-dimethylformamide (DMF, anhydrous 99.9%) were purchased from Alfa Aesar and used as received. Tris(trimethylsilyl) phosphine ((TMS)₃P, 98%, stored frozen), tris(dimethylamino)arsine (99%), and indium(iii) chloride (anhydrous, 99.999%) were purchased from Strem Chemicals and used as received. In general, we preferred salt precursors which are delivered as ~10 mesh beads in sealed ampules over fine mesh powders since the lower surface area minimized contamination with moisture and residual glovebox solvents. The beads were ground into fine powders as needed in an oven-dried mortar and pestle.

Synthesis of Li_2Se. Lithium selenide was synthesized from lithium triethylborohydride and selenium pellets as described previously. 44

InAs Nanocrystal Synthesis. Tetrahedron-shaped InAs nanocrystals were synthesized using modifications of established procedures. 11 Briefly 50 mL of OAm was degassed under vacuum in a 250 mL 3-neck round-bottom flask equipped with a condenser and 250 mL bump trap installed between the flask and condenser at 110 °C for several hours. Next 4 mmol of InCl₃ (884 mg) was added to the flask under flow of N_2 . The reaction was next heated to 130 °C under vacuum for 1 h. The flask was switched to N2 and heated to 290 °C. In a glovebox, 4 mmol of tris(dimethylamino)arsine was mixed with 5 mL of dry OAm and heated to 50 °C until bubbles stopped evolving. The As stock solution was injected into the flask at 280 °C, followed by injection of 4 mmol of DIBAL-H (4 mL of a 1 M stock solution in toluene). Caution: this rection is vigorous due to the evolution of gas from DIBAL-H and the high reaction temperature relative to the boiling point of toluene. The bump trap between the flask and condenser allowed the toluene to distill out of the reaction mixture. The reaction was held at 280 °C for 15 min, then cooled to room temperature under a stream of compressed air. The reaction flask was transferred to a glovebox, and the nanocrystals were precipitated by addition of anhydrous ethanol, centrifuged, and the supernatant discarded. The precipitate was dissolved in toluene, centrifuged to remove insoluble impurities which include amorphous As⁰. The nanocrystals were precipitated a second time using an ethanol/toluene nonsolvent pair and subsequently stored in hexane in a glovebox for future use.

Sphere-shaped InAs nanocrystals were synthesized according to established procedures. 45

InP Nanocrystal Synthesis. Tetrahedron-shaped and sphere-shaped InP nanocrystals were synthesized using recipes our group recently modified.²⁶

Molten Salt Preparation. All handing of salt precursors were carried out in a N2 glovebox. Care was taken to avoid exposing the salt precursors to a solvent vapor saturated glovebox atmosphere. KGaI₄ was prepared by loading "ultra-dry" KI and "ultra-dry" GaI3 in a 1:1 molar ratio into an oven-dried quartz ampule (9 mm outer diameter, 7 mm inner diameter, with an indentation to support a sealing plug above the sample), and a 6 mm diameter quartz plug was inserted. The ampule was attached to a vacuum transfer chuck to mount the ampule on a vacuum manifold without air exposure. The ampule was sealed under vacuum using a O₂/H₂ torch. Next the salts were melted in a vertical furnace at \sim 400 $^{\circ}$ C and after the salt melted the ampule was inverted several times followed by additional annealing for several hours to ensure complete reaction. The reaction was cooled to room temperature, brought into a N2 glovebox and the ampule was broken open in a mortar, the quartz pieces were mechanically separated, and the resulting salt was ground into a coarse powder and stored for future use. For KAlI₄, we found many commercial sources of AlI₃ were

contaminated with an I_2 impurity (resulting in a deep violet color of the melted salts). To avoid I_2 impurities, we sealed a 1:1 molar ratio of KI and AlI $_3$ and an aluminum metal slug in an ampule under vacuum. This sealed ampule was heated at $\sim\!400~^\circ\text{C}$ until a nearly colorless salt phase was observed, indicating all iodine had reacted with the excess aluminum metal, and this salt was recovered as described above. The KI/LiI eutectic mixture was prepared by grinding KI and LiI in the molar ratio 63:37 (melting point 250 $^\circ\text{C}$) in a mortar and pestle. The CsBr/KBr/LiBr eutectic mixture was prepared by grinding CsBr, LiBr, and KBr in the molar ratio of 25:19:56 (melting point 236 $^\circ\text{C}$) in a mortar and pestle. The CsI/KI/NaI eutectic mixture was prepared by grinding CsI, KI, and NaI in the molar ratio of 52:4:44 (melting point 407 $^\circ\text{C}$) 36 in a mortar and pestle.

Inorganic Ligand Exchange. To exchange the native organic ligands on InAs or InP nanocrystals for GaI_3 ligands, nanocrystals with their native surface ligands dissolved in ~15 mL of hexanes were layered on top of 5 mL a 0.05 M GaI_3 solution in DMF. This biphasic system was stirred for several hours until complete phase transfer of the nanocrystals to the DMF phase. Next the DMF phase was separated and washed with fresh hexanes. The nanocrystals were precipitated from the DMF solution by addition of 5 mL of acetonitrile (MeCN) and collected by centrifugation. The supernatant was discarded, and the nanocrystal pellet was suspended in fresh MeCN via vortexing followed by collection of the powder via centrifugation. Finally, the supernatant was discarded, and the nanocrystals were dried in a glovebox overnight in an open centrifuge tube for future use.

InAs nanocrystals with Se ligands were prepared based on modified literature procedures. Nanocrystals with their native organic ligands were dissolved in $\sim\!15$ mL of anhydrous hexanes and layered atop 5 mL of a 5 mg/mL solution of $\rm Li_2Se$ in formamide. This biphasic mixture was stirred for several hours until complete phase transfer of the nanocrystals to the lower formamide phase. The lower phase was isolated and washed 2 times with fresh anhydrous hexanes. The Secapped InAs nanocrystals were precipitated from the formamide phase using MeCN and recovered via centrifugation. The Se-capped InAs nanocrystal powder was washed 2 times by suspending the powder in $\sim\!5$ mL of MeCN by vigorous vortexing and centrifugation to recover the powder. Finally, the powder was dried in an open centrifuge tube in an $\rm N_2$ glovebox overnight.

Molten Salt Annealing of Nanocrystals. KGaI₄, KAlI₄ powders or mixtures thereof were finely ground in an oven-dried mortar and pestle in a N2 glovebox. Next the previously prepared GaI3- or Secapped InAs or InP nanocrystals were incorporated into the salt by gentle grinding with the mortar and pestle. Nanocrystals could be loaded in the salts with mass loading as high at 10 wt % nanocrystals without obvious negative impacts. The nanocrystal/salt mixture was loaded into a quartz ampule, air-free transferred to a vacuum manifold, and sealed under vacuum using an O2/H2 torch. Samples were annealed in a custom high-temperature heating block, which consisted of a 4-in. diameter cylindrical aluminum block with 8, 3/8in.-diameter 2.5-in.-deep holes drilled in a circle around a central thermocouple hole. The length of the sealed portion of the ampule was less than 2.5 in. ensuring the entire reaction volume was uniformly heated in the aluminum block. The block was wrapped in high-temperature heating tape (BriskHeat BWH) and several layers of insulation. The temperature was controlled using a PID temperature controller. The temperature in each hole was independently measured to be within ±2 °C of the set temperature. Samples were annealed for the desired time and temperature followed by removal from the heating block and allowing the sample cool to room temperature

Nanocrystal Recovery from Salt Matrix. The ampules were broken open in an N_2 glovebox, and the salt pellet embedded in the bottom of the ampule were placed in an oven-dried glass vial with a Teflon stir bar. 5 mL of MeCN (or a 3:2 mixture of MeCN:DMF for KAlI₄ containing salts) was added to the vial and stirred until the salt matrix dissolved. Next, the nanocrystals were separated by centrifugation and the supernatant discarded. The nanocrystal pellet was washed with additional MeCN (or 3:2 MeCN:DMF for KAlI₄

containing salt mixtures) and collected by centrifugation. The nanocrystal pellet was treated with a solution consisting of 50 μ L of OAm in 1 mL of toluene and stirred until the nanocrystals formed a colloidal solution. The nanocrystals were purified of excess ligand by precipitation with 5 mL of methyl acetate, centrifugation, and final dispersion in toluene for further characterization. All samples were stored in a glovebox and fresh aliquots were removed for characterization.

Nanocrystal Characterization. Powder X-ray diffraction patterns were collected on a Rigaku miniflex X-ray diffractometer. Samples were deposited on 511 Si low background substrates. lattice parameter and Scherrer size were determined by fitting the {111}, {220}, and {311} peaks to pseudo-Voigt functions to extract the peak width and position. The gallium composition was estimated by calculating the lattice parameter using the {111}, {220}, and {311} peaks and using a linear interpolation of the lattice parameters for the parent InAs and GaAs. TEM images were collected on an FEI Tecnai F30 microscope at 300 kV. X-ray fluorescence (XRF) analysis was performed with a benchtop Energy Dispersive Rigaku NEX DE VS Xray fluorimeter equipped with a Peltier cooled FAST SDD Silicon Drift Detector. All analyses were carried out under He atmosphere to increase sensitivity for lighter elements. Elemental ratios were determined using the standardless thin films fundamental parameters method as programmed in QuantEZ software provided by Rigaku, using the standard Rigaku calibration protocols. All samples were measured on a PTFE substrate to avoid the large Si K_a peak which interferes with the aluminum and phosphorus K_{α} peak.

High Temperature UV-vis Measurements. Light from a stabilized tungsten halogen lamp (Thor Laboratories SLS201L) was passed through a temperature balancing filter (Thor Laboratories FTG200) and coupled into a 1000 μm diameter optical fiber. The output of the fiber was focused onto the center of a 9 mm O.D., 7 mm I.D. quartz ampule housed in a custom machined aluminum heating block using an adjustable fiber collimator. The heating block was heated with a 150 W swaged cartridge heater controlled by a temperature controller and thermocouple. The sample temperature was independently calibrated using a sand filled ampule and a second thermocouple. The light was transmitted through the sample and collected into a second fiber with a high NA fiber collimator (Thor Laboratories F950SMA-A). Spectra were measured using an Ocean Insight HR4PRO spectrometer. To collect absorption spectra, first the white light spectrum was collected after passing through a molten KI/ LiI eutectic sample. Then the sample of interest was placed in the heating block at the desired temperature to measure absorption spectra. All spectral calculations were handled using the Ocean View software. See Figure S20 for more details.

Ambient and High Temperature Raman Measurements. All Raman measurements were performed using a HORIBA LabRAM HR Evolution Confocal Raman Microscope. All room temperature measurements were performed using a 532 nm laser source, an ultralow frequency filter enabling measurement of Raman shifts as low as 10 cm⁻¹, an 1800 grooves/mm grating (resolution ~1 cm⁻¹) and detected using a Horiba Synapse OE-CCD. For high-temperature Raman experiments, the KGaI4-based samples were measured with the same 532 nm laser. Due to strong absorption of the 532 nm laser, the GaI₃ and GaI₃/KI [65:35 mol %] eutectic at high temperatures were measured with a 633 nm laser and a standard filter enabling measurement of Raman shifts to 50 cm⁻¹, an 1800 grooves/mm grating (resolution ~1 cm⁻¹), and detected using a Horiba Synapse OE-CCD. The spectrometer was calibrated using the Horiba LabSpec software using a Si (111) reference sample for all measurements. For room-temperature measurements, a sealed quartz ampule (9 mm O.D., 7 mm I.D.) with a solid salt plug at the bottom was placed horizontally on the microscope stage. The laser was focused on the center of the curved ampule using a 10× objective to collect spectra. For high-temperature measurements, a custom optical path turned the laser output of the Raman microscope 90 deg and focused the light into a sealed quartz ampule held vertically in an aluminum heating block, which was used to heat the salt samples (see Figure S21 for more details).

Note on Nomenclature. Rigorous convention for III–V alloy systems suggests that the metal and pnictide constituents are listed in increasing atomic number respectively (e.g., GaInAs, InPAs, etc.). However, often the InGaAs is used interchangeably with the rigorous (i.e., GaInAs) convention. For this work, we deviate from the rigorous convention and always list indium first since the resulting $In_{1-x}Ga_xPn$ notation is consistent with our previous publications and emphasizes that we start with InPn and as gallium is incorporated, indium is removed.

ASSOCIATED CONTENT

5 Supporting Information

The Supporting Information is available free of charge at https://pubs.acs.org/doi/10.1021/acsnano.3c09490.

Additional photos of molten salt phase separation; additional Raman characterization of molten salt solvents; additional UV—vis absorption spectroscopy of molten salt solvents; Small angle X-ray scattering of nanocrystal colloids; additional powder X-ray diffraction characterization of III—V nanocrystals; additional TEM characterization of III—V nanocrystals and photos of experimental setups (PDF)

AUTHOR INFORMATION

Corresponding Author

Dmitri V. Talapin — Department of Chemistry, James Franck Institute, and Pritzker School of Molecular Engineering, University of Chicago, Chicago, Illinois 60637, United States; Center for Nanoscale Materials, Argonne National Laboratory, Argonne, Illinois 60439, United States; orcid.org/0000-0002-6414-8587; Email: dvtalapin@uchicago.edu

Authors

Justin C. Ondry — Department of Chemistry, James Franck Institute, and Pritzker School of Molecular Engineering, University of Chicago, Chicago, Illinois 60637, United States; Occid.org/0000-0001-9113-3420

Aritrajit Gupta — Department of Chemistry, James Franck Institute, and Pritzker School of Molecular Engineering, University of Chicago, Chicago, Illinois 60637, United States; © orcid.org/0000-0001-9406-8986

Zirui Zhou – Department of Chemistry, James Franck Institute, and Pritzker School of Molecular Engineering, University of Chicago, Chicago, Illinois 60637, United States

Jun Hyuk Chang – Department of Chemistry, James Franck Institute, and Pritzker School of Molecular Engineering, University of Chicago, Chicago, Illinois 60637, United States

Complete contact information is available at: https://pubs.acs.org/10.1021/acsnano.3c09490

Notes

The authors declare no competing financial interest.

ACKNOWLEDGMENTS

We are grateful to Dr. Andrew Nelson for a critical reading and editing of the manuscript. We are thankful to Dr. Justin Jureller for help in designing and implementing the high-temperature Raman measurement apparatus used in this work. The work on QD synthesis was supported by the Samsung QD Cluster Collaboration. Advanced characterization of colloidal dispersions in molten inorganic salts was supported by the National Science Foundation under award number DMR-

2019444. This work made use of the shared facilities at the University of Chicago Materials Research Science and Engineering Center, supported by National Science Foundation under award number DMR-2011854. Work performed at the Center for Nanoscale Materials, a U.S. Department of Energy Office of Science User Facility, was supported by the U.S. DOE, Office of Basic Energy Sciences, under Contract No. DE-AC02-06CH11357.

REFERENCES

- (1) Kovalenko, M. V.; Manna, L.; Cabot, A.; Hens, Z.; Talapin, D. V.; Kagan, C. R.; Klimov, V. I.; Rogach, A. L.; Reiss, P.; Milliron, D. J.; Guyot-Sionnnest, P.; Konstantatos, G.; Parak, W. J.; Hyeon, T.; Korgel, B. A.; Murray, C. B.; Heiss, W. Prospects of Nanoscience with Nanocrystals. *ACS Nano* **2015**, *9* (2), 1012–1057.
- (2) Nguyen, Q. N.; Wang, C.; Shang, Y.; Janssen, A.; Xia, Y. Colloidal Synthesis of Metal Nanocrystals: From Asymmetrical Growth to Symmetry Breaking. *Chem. Rev.* **2023**, *123*, 3693.
- (3) Van den Eynden, D.; Pokratath, R.; De Roo, J. Nonaqueous Chemistry of Group 4 Oxo Clusters and Colloidal Metal Oxide Nanocrystals. *Chem. Rev.* **2022**, *122* (11), 10538–10572.
- (4) Akkerman, Q. A.; Rainò, G.; Kovalenko, M. V.; Manna, L. Genesis, Challenges and Opportunities for Colloidal Lead Halide Perovskite Nanocrystals. *Nat. Mater.* **2018**, *17* (5), 394–405.
- (5) Joo, J.; Na, H. B.; Yu, T.; Yu, J. H.; Kim, Y. W.; Wu, F.; Zhang, J. Z.; Hyeon, T. Generalized and Facile Synthesis of Semiconducting Metal Sulfide Nanocrystals. *J. Am. Chem. Soc.* **2003**, *125* (36), 11100–11105
- (6) Kim, Y.; Chang, J. H.; Choi, H.; Kim, Y.-H.; Bae, W. K.; Jeong, S. III–V Colloidal Nanocrystals: Control of Covalent Surfaces. *Chem. Sci.* **2020**, *11* (4), 913–922.
- (7) Murray, C. B.; Norris, D. J.; Bawendi, M. G. Synthesis and Characterization of Nearly Monodisperse CdE (E = Sulfur, Selenium, Tellurium) Semiconductor Nanocrystallites. *J. Am. Chem. Soc.* **1993**, *115* (19), 8706–8715.
- (8) Yin, Y.; Alivisatos, A. P. Colloidal Nanocrystal Synthesis and the Organic–Inorganic Interface. *Nature* **2005**, 437 (7059), 664–670.
- (9) Nguyen, H. A.; Dixon, G.; Dou, F. Y.; Gallagher, S.; Gibbs, S.; Ladd, D. M.; Marino, E.; Ondry, J. C.; Shanahan, J. P.; Vasileiadou, E. S.; Barlow, S.; Gamelin, D. R.; Ginger, D. S.; Jonas, D. M.; Kanatzidis, M. G.; Marder, S. R.; Morton, D.; Murray, C. B.; Owen, J. S.; Talapin, D. V.; Toney, M. F.; Cossairt, B. M. Design Rules for Obtaining Narrow Luminescence from Semiconductors Made in Solution. *Chem. Rev.* 2023, 123 (12), 7890–7952.
- (10) Kortan, A. R.; Hull, R.; Opila, R. L.; Bawendi, M. G.; Steigerwald, M. L.; Carroll, P. J.; Brus, L. E. Nucleation and Growth of CdSe on ZnS Quantum Crystallite Seeds, and Vice Versa, in Inverse Micelle Media. J. Am. Chem. Soc. 1990, 112 (4), 1327–1332.
- (11) Srivastava, V.; Janke, E. M.; Diroll, B. T.; Schaller, R. D.; Talapin, D. V. Facile, Economic and Size-Tunable Synthesis of Metal Arsenide Nanocrystals. *Chem. Mater.* **2016**, 28 (18), 6797–6802.
- (12) Srivastava, V.; Dunietz, E.; Kamysbayev, V.; Anderson, J. S.; Talapin, D. V. Monodisperse InAs Quantum Dots from Aminoarsine Precursors: Understanding the Role of Reducing Agent. *Chem. Mater.* **2018**, *30* (11), 3623–3627.
- (13) Tessier, M. D.; De Nolf, K.; Dupont, D.; Sinnaeve, D.; De Roo, J.; Hens, Z. Aminophosphines: A Double Role in the Synthesis of Colloidal Indium Phosphide Quantum Dots. *J. Am. Chem. Soc.* **2016**, 138 (18), 5923–5929.
- (14) Won, Y.-H.; Cho, O.; Kim, T.; Chung, D.-Y.; Kim, T.; Chung, H.; Jang, H.; Lee, J.; Kim, D.; Jang, E. Highly Efficient and Stable InP/ZnSe/ZnS Quantum Dot Light-Emitting Diodes. *Nature* **2019**, *575* (7784), *634*–*638*.
- (15) Hanifi, D. A.; Bronstein, N. D.; Koscher, B. A.; Nett, Z.; Swabeck, J. K.; Takano, K.; Schwartzberg, A. M.; Maserati, L.; Vandewal, K.; van de Burgt, Y.; Salleo, A.; Alivisatos, A. P. Redefining Near-Unity Luminescence in Quantum Dots with Photothermal Threshold Quantum Yield. *Science* **2019**, 363 (6432), 1199–1202.

- (16) Chen, O.; Zhao, J.; Chauhan, V. P.; Cui, J.; Wong, C.; Harris, D. K.; Wei, H.; Han, H.-S.; Fukumura, D.; Jain, R. K.; Bawendi, M. G. Compact High-Quality CdSe-CdS Core-Shell Nanocrystals with Narrow Emission Linewidths and Suppressed Blinking. *Nat. Mater.* **2013**, *12* (5), 445–451.
- (17) Srivastava, V.; Liu, W.; Janke, E. M.; Kamysbayev, V.; Filatov, A. S.; Sun, C.-J.; Lee, B.; Rajh, T.; Schaller, R. D.; Talapin, D. V. Understanding and Curing Structural Defects in Colloidal GaAs Nanocrystals. *Nano Lett.* **2017**, *17* (3), 2094–2101.
- (18) Beberwyck, B. J.; Alivisatos, A. P. Ion Exchange Synthesis of III–V Nanocrystals. J. Am. Chem. Soc. 2012, 134 (49), 19977–19980.
- (19) Lauth, J.; Strupeit, T.; Kornowski, A.; Weller, H. A Transmetalation Route for Colloidal GaAs Nanocrystals and Additional III–V Semiconductor Materials. *Chem. Mater.* **2013**, 25 (8), 1377–1383.
- (20) Gupta, S. K.; Mao, Y. Recent Developments on Molten Salt Synthesis of Inorganic Nanomaterials: A Review. *J. Phys. Chem. C* **2021**, 125 (12), 6508–6533.
- (21) Liu, X.; Fechler, N.; Antonietti, M. Salt Melt Synthesis of Ceramics, Semiconductors and Carbon Nanostructures. *Chem. Soc. Rev.* 2013, 42 (21), 8237.
- (22) Zhang, H.; Dasbiswas, K.; Ludwig, N. B.; Han, G.; Lee, B.; Vaikuntanathan, S.; Talapin, D. V. Stable Colloids in Molten Inorganic Salts. *Nature* **2017**, *542* (7641), 328–331.
- (23) Srivastava, V.; Kamysbayev, V.; Hong, L.; Dunietz, E.; Klie, R. F.; Talapin, D. V. Colloidal Chemistry in Molten Salts: Synthesis of Luminescent $In_{1-x}Ga$ $_xP$ and $In_{1-x}Ga$ $_xAs$ Quantum Dots. *J. Am. Chem. Soc.* **2018**, *140* (38), 12144–12151.
- (24) Hudson, M. H.; Gupta, A.; Srivastava, V.; Janke, E. M.; Talapin, D. V. Synthesis of $In_{1-x}Ga$ _xP Quantum Dots in Lewis Basic Molten Salts: The Effects of Surface Chemistry, Reaction Conditions, and Molten Salt Composition. *J. Phys. Chem. C* **2022**, *126* (3), 1564–1580.
- (25) Gupta, A.; Ondry, J. C.; Lin, K.; Chen, Y.; Hudson, M. H.; Chen, M.; Schaller, R. D.; Rossini, A. J.; Rabani, E.; Talapin, D. V. Composition-Defined Optical Properties and the Direct-to-Indirect Transition in Core—Shell In_{1-x} Ga_xP/ZnS Colloidal Quantum Dots. *J. Am. Chem. Soc.* **2023**, *145* (30), 16429–16448.
- (26) Gupta, A.; Ondry, J. C.; Chen, M.; Hudson, M. H.; Coropceanu, I.; Sarma, N. A.; Talapin, D. V. Diffusion-Limited Kinetics of Isovalent Cation Exchange in III–V Nanocrystals Dispersed in Molten Salt Reaction Media. *Nano Lett.* **2022**, 22 (16), 6545–6552.
- (27) Kamysbayev, V.; Srivastava, V.; Ludwig, N. B.; Borkiewicz, O. J.; Zhang, H.; Ilavsky, J.; Lee, B.; Chapman, K. W.; Vaikuntanathan, S.; Talapin, D. V. Nanocrystals in Molten Salts and Ionic Liquids: Experimental Observation of Ionic Correlations Extending beyond the Debye Length. *ACS Nano* **2019**, *13* (5), 5760–5770.
- (28) Dirin, D. N.; Dreyfuss, S.; Bodnarchuk, M. I.; Nedelcu, G.; Papagiorgis, P.; Itskos, G.; Kovalenko, M. V. Lead Halide Perovskites and Other Metal Halide Complexes As Inorganic Capping Ligands for Colloidal Nanocrystals. *J. Am. Chem. Soc.* **2014**, *136* (18), 6550–6553.
- (29) Nag, A.; Kovalenko, M. V.; Lee, J.-S.; Liu, W.; Spokoyny, B.; Talapin, D. V. Metal-Free Inorganic Ligands for Colloidal Nanocrystals: S 2 –, HS $^-$, Se 2 –, HSe $^-$, Te 2 –, HTe $^-$, TeS $_3$ 2 –, OH $^-$, and NH $_2$ $^-$ as Surface Ligands. *J. Am. Chem. Soc.* **2011**, 133 (27), 10612–10620.
- (30) Amon, A.; Sener, M. E.; Rosu-Finsen, A.; Hannon, A. C.; Slater, B.; Salzmann, C. G. Preparation and Structure of the Ion-Conducting Mixed Molecular Glass Ga ₂ I _{3.17}. *Inorg. Chem.* **2021**, *60* (9), 6319–6326.
- (31) Taylor, M. J. Spectroscopic Studies of Gallium Complexes in Solution. *Polyhedron* **1990**, *9* (2), 207–214.
- (32) Waterworth, L. G.; Worrall, I. J. Raman Studies into the Constitution of Gallium Iodides of Intermediate Composition. *J. Inorg. Nucl. Chem.* **1973**, 35 (5), 1535–1537.
- (33) Moore, R. H. Immiscibility Gap in the System: LiCl-KCl-AlCl3. *J. Chem. Eng. Data* **1963**, 8 (2), 164–167.

- (34) Pearson, R. G. Absolute Electronegativity and Hardness: Application to Inorganic Chemistry. *Inorg. Chem.* **1988**, 27 (4), 734–740.
- (35) Pearson, R. G. Absolute Electronegativity and Hardness Correlated with Molecular Orbital Theory. *Proc. Natl. Acad. Sci. U. S. A.* **1986**, 83 (22), 8440–8441.
- (36) Janz, G. J.; Allen, C. B.; Downey, J. R.; Tomkins, R. P. T. Physical Properties Data Compilations Relevant to Energy Storage. I. Molten Salts: Eutectic Data; United States, 1978. https://www.osti.gov/biblio/6451622 (accessed Dec. 6, 2023).
- (37) Mascherpa-Corral, D.; Potier, A. L'ion lineaire heptaiododigallate dans les cristaux RbGa2I7 et CsGa2I7. *J. Inorg. Nucl. Chem.* **1976**, 38 (2), 211–213.
- (38) Alvarenga, A. D.; Saboungi, M.-L.; Curtiss, L. A.; Grimsditch, M.; McNeil, L. E. Structure and Dynamics of Molten Aluminium and Gallium Trihalides: II. Raman Spectroscopy and *Ab Initio* Calculations. *Mol. Phys.* **1994**, *81* (2), 409–420.
- (39) Nakamoto, K. Infrared and Raman Spectra of Inorganic and Coordination Compounds, 6th ed.; Wiley: Hoboken, NJ, 2009.
- (40) Amon, A.; Sener, M. E.; Rosu-Finsen, A.; Hannon, A. C.; Slater, B.; Salzmann, C. G. Preparation and Structure of the Ion-Conducting Mixed Molecular Glass Ga2I3.17. *Inorg. Chem.* **2021**, *60* (9), 6319–6326.
- (41) Crystal Structure of Sodium Tetraiodoaluminate (III), NaAlI4. Z. Für Krist. Cryst. Mater. 1994, 209 (6), 544–544. .
- (42) Materials Data on NaAlI4 by Materials Project; mp-29395; Lawrence Berkeley National Lab. (LBNL): Berkeley, CA. LBNL Materials Project, 2020. DOI: 10.17188/1203770.
- (43) Begun, G. M.; Boston, C. R.; Torsi, G.; Mamantov, G. Raman Spectra of Molten Aluminum Trihalide-Alkali Halide Systems. *Inorg. Chem.* **1971**, *10* (5), 886–889.
- (44) Beecher, A. N.; Yang, X.; Palmer, J. H.; LaGrassa, A. L.; Juhas, P.; Billinge, S. J. L.; Owen, J. S. Atomic Structures and Gram Scale Synthesis of Three Tetrahedral Quantum Dots. *J. Am. Chem. Soc.* **2014**, *136* (30), 10645–10653.
- (45) Kim, T.; Park, S.; Jeong, S. Diffusion Dynamics Controlled Colloidal Synthesis of Highly Monodisperse InAs Nanocrystals. *Nat. Commun.* **2021**, *12* (1), 3013.